molecular structure and multimer formation of adiponectin. J Biol Chem 2003;278:40352–63.
7. Hada Y, Yamauchi T, Waki H, Tsuchida A, Hara K, Yago H, et al. Selective purification and characterization of adiponectin multimer species from human plasma. Biochem Biophys Res Commun 2007;356:487–93.
8. Pajvani UB, Hawkins M, Combs TP, Rajala MW, Doebber T, Berger JP, et al. Complex distribution, not absolute amount of adiponectin, correlates with thiazolidinedione-mediated improvement in insulin sensitivity. J Biol Chem 2004;279:12152–62.
9. Hara K, Horikoshi M, Yamauchi T, Yago H, Miyazaki O, Ebinuma H, et al. Measurement of the high-molecular-weight form of adiponectin in plasma is useful for the prediction of insulin resistance and metabolic syndrome. Diabetes Care 2006;29:1357–62.
10. Ebinuma H, Miyazaki O, Yago H, Hara K, Yamauchi T, Kadowaki T. A novel ELISA system for selective measurement of human adiponectin multimers by using proteases. Clin Chim Acta 2006;372:47–53.
11. Yoshida H. [Histological view of ethics in medicine and handling of residual samples in clinical laboratories.] Rinsho Byori 2004;52:231–5.
12. Numata Y, Morita A, Kosugi Y, Shibata K, Takeuchi N, Uchida K. New sandwich ELISA for human urinary N-acetyl-beta-D-glucosaminidase isoenzyme B as a useful clinical test. Clin Chem 1997;43:569–74.
13. Wang Y, Xu A, Knight C, Xu LY, Cooper GJ. Hydroxylation and glycosylation of the four conserved lysine residues in the collagenous domain of adiponectin: potential role in the modulation of its insulin-sensitizing activity. J Biol Chem 2002;277:19521–9.
14. Kusminski CM, McTernan PG, Schraw T, Kos K, O'Hare JP, Ahima R, et al. Adiponectin complexes in human cerebrospinal fluid: distinct complex distribution from serum. Diabetologia 2007;50:634–42.

Previously published online at DOI: 10.1373/clinchem.2007.085654

Expanded Instrument Comparison of Amplicon DNA Melting Analysis for Mutation Scanning and Genotyping

Mark G. Herrmann,[1*] *Jacob D. Durtschi,*[1] *Carl T. Wittwer,*[1,2] *and Karl V. Voelkerding*[1,2] ([1] Institute for Clinical and Experimental Pathology, ARUP, Salt Lake City, UT; [2] Department of Pathology, University of Utah School of Medicine, Salt Lake City, UT; * address correspondence to this author at: ARUP Laboratories, 500 Chipeta Way, Salt Lake City, UT 84108; fax 801-584-5114, e-mail mark.herrmann@aruplab.com)

Background: **Additional instruments have become available since instruments for DNA melting analysis of PCR products for genotyping and mutation scanning were compared. We assessed the performance of these new instruments for genotyping and scanning for mutations.**

Methods: **A 110-bp fragment of the β-globin gene including the sickle cell anemia locus (*HBB* c. 20A>T) was amplified by PCR in the presence of LCGreen Plus or SYBR Green I. Amplicons of 4 different genotypes [wild-type, homozygous, and heterozygous *HBB* c. 20A>T and double-heterozygote *HBB* c. (9C>T; 20A>T)] were melted on 7 different instruments [Applied Biosystems 7300, Corbett Life Sciences Rotor-Gene 6500HRM, Eppendorf Mastercycler RealPlex4S, Idaho Technology LightScanner (384 well), Roche LightCycler 480 (96 and 384 well) and Stratagene Mx3005p] at a rate of 0.61 °C/s or when this was not possible, at 0.50 °C steps. We evaluated the ability of each instrument to genotype by melting temperature (T_m) and to scan for heterozygotes by curve shape.**

Results: **The ability of most instruments to accurately genotype single-base changes by amplicon melting was limited by spatial temperature variation across the plate (SD of T_m = 0.020 to 0.264 °C). Other variables such as data density, signal-to-noise ratio, and melting rate also affected heterozygote scanning.**

Conclusions: **Different instruments vary widely in their ability to genotype homozygous variants and scan for heterozygotes by whole amplicon melting analysis. Instruments specifically designed for high-resolution melting, however, displayed the least variation, suggesting better genotyping accuracy and scanning sensitivity and specificity.**

Melting curve analysis has grown in sophistication from genotyping single-base variants with fluorescence resonance energy transfer probes *(1)* to inferring and differentiating sequence homologies through high-resolution amplicon melting with DNA binding dyes *(2–4)*. These advanced techniques are already being adapted to existing real-time PCR instruments. In our prior studies *(5, 6)*, we evaluated the melting capabilities of 9 melting instruments found in our laboratory. These instruments varied in ability to detect homozygous mutants as well as to identify single- and double-heterozygous samples. The ability to differentiate complex melting species depends on the quality of the melting curve generated. Since our initial reports, 7 additional instruments have become available for genotyping and heterozygote scanning. Understanding the melting capabilities of these instruments should guide the appropriate use of different techniques.

As previously described *(5, 6)*, a 110-bp fragment of the β-globin gene including the sickle cell anemia locus (*HBB* c. 20A>T) was amplified by PCR in the presence of a DNA binding dye. A single patient sample of each genotype [wild-type, homozygous, and heterozygous *HBB* c. 20A>T and double-heterozygote *HBB* c. (9C>T; 20A>T)] were amplified, pooled by genotype, and reallocated for instrument evaluation. Melting curves were obtained with the Applied Biosystems 7300, Corbett Life Science Rotor-Gene™ 6500HRM, Eppendorf Mastercycler® RealPlex4S, Idaho Technology LightScanner® (384 well), Roche LightCycler® 480 (96- and 384-well models), and Stratagene Mx3005p™. Melting curves were obtained at 0.1 °C/s if possible. For instruments able to perform only step monitoring, the melting cycle was monitored at 10 acquisitions/°C with a 10-s hold. A single 96/384-well plate or 72-sample rotor containing homogenous wild-type amplicon and LCGreen® Plus (Idaho Technology) were used to determine temperature homogeneity [expressed as the melting temperature (T_m) SD], melting curve superimposability (expressed as the temperature-shifted T_m SD), signal-to-noise ratio, data density, and, for the heat block instruments, dynamic thermal profiles. Because of spectral incompatibilities with LCGreen Plus,

SYBR Green I (Invitrogen) was used with the Stratagene's Mx3005p.

Heterozygote scanning was also evaluated by melting each of the 4 genotypes in triplicate. For heat block instruments, the amplicons were placed in identical positions randomly dispersed across the plate, with an equal volume of water filling the intervening spaces. The resulting melting curves were temperature-shifted for resolving single- and double-heterozygous samples.

The normalized melting curves are shown in Fig. 1A. The apparent temperature variation within a genotype was highly dependent on the instrument used. After temperature shifting, the T_m variation within a genotype was usually decreased (Fig. 1B), particularly in the case of the 7300 and LC480 instruments, for which temperature shifting enabled heterozygote differentiation. The displacement of the double heterozygote was so great that it was distinguishable in all cases, but accurate detection of the single heterozygote was not achieved with all instruments.

Table 1 shows instrument variables and measured T_m SDs compiled from this and prior studies *(5, 6)*. The T_m SDs directly affect the ability to separate different homozygous melting curves. The main contributing variable appears to be temperature homogeneity. As seen previously, air-based instruments and instruments with individual sample temperature control have lower T_m SDs (0.018–0.065) than their heat-block counterparts (0.092–0.274). Block systems with thermal electric heaters had lower T_m SDs (0.092–0.102) then Peltier-based systems (0.117–0.274). The dynamic melting profile for the 96-well and 384-well heat blocks are shown in Fig. 1C. Thermal edge effects and the Peltier configuration can be inferred from the thermal maps of the heat block instruments.

Genotyping single-base variants with fluorescent probes usually results in T_m differences for the matched and mismatched species of 4–10 °C. All the instruments studied are capable of genotyping at this level of resolution. When genotyping is performed by amplicon melting, however, T_m differences are much smaller. The mean T_m difference of homozygotes of class 1 and class 2 single-nucleotide polymorphisms (SNPs) was 1 °C, and almost all have a T_m difference >0.5 °C *(7)*. In 8 of the instruments, estimated error rates were <1% at this degree of resolution (SD <0.109) *(5)*. When the melting difference was decreased to >0.25 °C, as in typical class 3 and class 4 SNPs, only 5 of the instruments evaluated had an estimated error rate of <1% (SD >0.054).

Different homozygotes each produce only a single homoduplex species. Therefore, genotyping by T_m (determined as the temperature at 50% of the normalized fluorescence) is straightforward and has an accuracy directly correlated to temperature homogeneity. The T_m variation of block-based systems is greater than that for air-based or individual sample systems. This variation is attributable to difficulties in uniformly heating large metal blocks and assigning a single temperature to represent the entire block. The thermal control of multiple samples is improved with air-based systems, for which rapid mixing forces temperature homogeneity. Alternatively, single-sample systems also fared well, because spatial temperature homogeneity is not a concern, allowing better temperature control and measurement.

Detection of heterozygous samples by amplicon melting is more complex than homozygote differentiation. Heterozygotes differ primarily in melting curve shape rather than absolute T_m. These differences are often visualized after temperature shifting to superimpose the curves, allowing easy visualization and grouping by melting curve shape. For any heterozygous sample, the resulting melting curve is a combination of 2 homoduplexes and 2 heteroduplexes that form as the samples are cooled. Mismatched duplexes melt at lower temperatures than homoduplexes. For example, PCR of the single heterozygote (*HBB* c. 20A>T) produces duplexes with predicted T_ms *(7)* of 85.89 and 85.80 °C for the homoduplexes and 85.11 and 85.10 °C for the heteroduplexes. The resulting melting curves on most instruments show 2 melting regions, a lower temperature region of heteroduplex melting and a higher region of homoduplex melting. The double-heterozygous sample [*HBB* c. (9C>T; 20A>T)] again is composed of 2 heteroduplexes with predicted T_ms of 84.41 and 84.51 °C and 2 homoduplexes with predicted T_ms of 85.36 and 85.89 °C. In this case, the 2 homoduplex species are separated by 0.53 °C and can be distinguished on some instruments. The ability to resolve subtleties in the melting curve requires more than a single T_m for proper identification. The melting curve shape of heterozygotes depends on the number of discrete melting populations, the sharpness of each transition, and the different stabilities of each species.

About half of the instruments surveyed performed heterozygote scanning well. Multiple variables affect the quality of DNA melting curves, including data density, signal-to-noise ratio, and melting rate. For example, increasing the data density beyond 10 points/°C allows for more melting information to be displayed and potentially the resolution of more duplex species. In addition, the 3 melting domains of the double heterozygotes were easier to resolve in melting curves with higher signal-to-noise ratios and good superimposability (low temperature-shifted T_m SD). Improved resolution also becomes important in recognizing unknown variants that occur within the amplicon studied *(8)*. Prior reports suggest that better heteroduplex detection is obtained at faster melting rates and higher signal-to-noise ratios *(9)*. Although a general correlation with these factors was observed, the significance of each factor and their interactions will require further study.

Limitations of the current study include the assumption that each instrument and its performance are typical. For a few instruments additional runs were performed and did not significantly differ from those reported (data

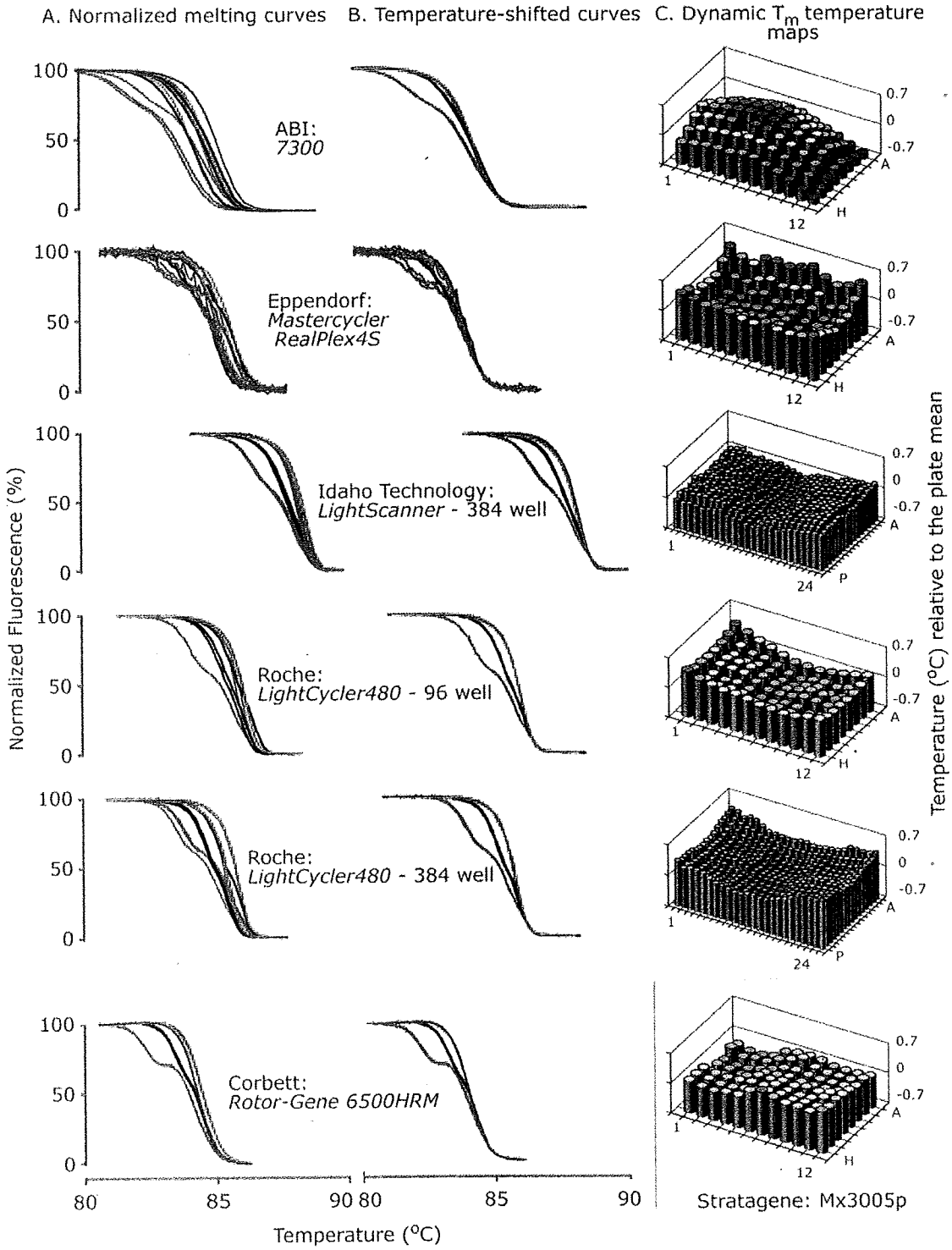

Fig. 1. Normalized and temperature-shifted melting curves of a 110-bp β-globin amplicon and the associated thermal profiles of heat block instruments.

Each genotype was melted and displayed in triplicate on the different instruments. Melting curves for the homozygous wild type are shown in *green*, homozygous mutant (c. 20A>T) in *red*, the single-heterozygous mutant (c. 20A>T) in *black*, and the double-heterozygote mutant [c. (9C>T; 20A>T)] in *blue*. (*A*), normalized melting curves of each instrument studied. (*B*), temperature-shifted melting curves used for heterozygote scanning. (*C*), the dynamic melting profile of all plate instruments referenced to the mean T_m of the wild-type amplicon. LCGreen Plus was used as the dye, except on the Stratagene Mx3005p, which required use of SYBR Green I.

Table 1. Instrument and sample characteristics.

Instrument	Sample and thermal format	Acquisition mode	Data points/°C	Melting rates,[a] °C/s	Melting time, min	S/N[b]	T_m SD_n, °C[c]	T_m SD_{ts}, °C[d]	n	T_m range,[e] °C
LCGreen Plus-compatible										
ABI: 7000	96-well plate, Peltier	Cont.	3.1	0.022	27.0	560	0.117	0.065	96	0.66
ABI: 7300	96-well plate, Peltier	Cont.	2.7	0.036	16.0	[f]	0.263	[f]	96	1.02
Bio-Rad: iCycler	96-well plate, Peltier	Step	10	0.009	65.0	410	0.173	0.064	96	1.10
Cepheid: SmartCycler	1 square tube, thermal electric/air	Cont.	10	0.100	5.8	310	0.065	0.051	32	0.22
Corbett: Rotor-Gene 3000	72 tubes, circulating air	Step	10	0.008	73.0	180	0.045	0.051	72	0.19
Corbett: Rotor-Gene 6500HRM	72 tubes, circulating air	Step	10	0.006	97.0	300	0.020	0.028	72	0.09
Eppendorf: Mastercycler RealPlex4S	96-well plate, Peltier	Cont.	10	0.012	49.0	90	0.226	0.042	96	0.87
Idaho Technology: HR-1	1 glass capillary, thermal electric	Cont.	200	0.100	5.8	3500	0.018	0.012	32	0.06
Idaho Technology: LightScanner (384)	384-well plate, thermal electric	Cont.	12	0.105	6.0	520	0.096	0.024	384	0.45
Idaho Technology: LightScanner (96)	96-well plate, thermal electric	Cont.	14	0.100	5.8	1800	0.092	0.013	96	0.35
Roche: LightCycler 1.2	32 glass capillaries, circulating air	Cont.	5.2	0.100	5.9	260	0.045	[f]	32	0.19
Roche: LightCycler 2.0	32 glass capillaries, circulating air	Cont.	4.1	0.100	6.5	490	0.047	[f]	32	0.18
Roche: LightCycler 480 (384)	384-well plate, Peltier	Cont.	10	0.090	7.3	460	0.160	0.017	384	0.71
Roche: LightCycler 480 (96)	96-well plate, Peltier	Cont.	10	0.110	6.3	670	0.144	0.014	96	0.67
SYBR Green I-compatible										
ABI: 7900HT	96-well plate	Cont.	4.2	0.014	42.0	180	0.274	[f]	96	1.24
Stratagene: Mx3005p	96-well plate	Cont.	1.9	0.030	19.0	60	0.139	0.090	96	0.61
		Step	10	0.009	65.0	60	0.159	0.060	96	0.50

[a] Observed melting rates (programmed at 0.1 °C/s when possible).
[b] S/N, signal-to-noise ratio as determined in Ref. 1.
[c] SD of the T_m within a genotype for normalized melting curves (relevant to genotyping and instrument temperature homogeneity).
[d] SD of the T_m within a genotype after temperature-shifting (relevant to heterozygote scanning and melting curve superimposability).
[e] Temperature range of T_m based on n values.
[f] Calculation not possible.

not shown). Another concern is that the number of samples studied was influenced by the sample capacity of each instrument (96 or 384 for plates and 72 or 32 for rotors). These within-run variations were compared to 32 interrun variances on single sample instruments.

Melting curve analysis with saturating DNA dyes is a simple method for genotyping and scanning *(7)*. Homozygous samples can often be genotyped by an absolute change in T_m *(10)*, while heterozygous samples can be identified through changes in the shape of the melting curve *(11, 12)*. Recently, internal temperature controls have been used to correct for T_m variation seen in low-resolution instruments *(13–15)*. These controls provide a reference to correctly genotype homozygous alleles regardless of the temperature homogeneity of the system. The detection of subtle sequence changes for variant scanning will continue to rely on the resolution of melting instruments.

Grant/funding support: Applied Biosystems, Corbett Life Science, Eppendorf, Idaho Technology, and Stratagene provided access to demonstration instruments, which were temporarily placed in the ARUP laboratory for this evaluation. The project was otherwise funded solely by ARUP Laboratories.
Financial disclosures: Aspects of melting analyses are covered by issued and pending patents owned by the University of Utah and licensed to Idaho Technology. C.T.W. holds equity interest in Idaho Technology.
Acknowledgments: We thank Applied Biosystems, Corbett Life Science, Eppendorf, Idaho Technology, and Stratagene for technical support during this evaluation and thank the reviewers and editors for valuable comments.

References

1. Lay MJ, Wittwer CT. Real-time fluorescence genotyping of factor V Leiden during rapid-cycle PCR. Clin Chem 1997;43:2262–7.
2. Krypuy M, Newnham GM, Thomas DM, Conron M, Dobrovic A. High resolution melting analysis for the rapid and sensitive detection of mutations in clinical samples: KRAS codon 12 and 13 mutations in non-small cell lung cancer. BMC Cancer 2006;6:295.
3. Reed GH, Wittwer CT. Sensitivity and specificity of single-nucleotide polymorphism scanning by high-resolution melting analysis. Clin Chem 2004; 50:1748–54.
4. Zhou L, Vandersteen J, Wang L, Fuller T, Taylor M, Palais B, et al. High-resolution DNA melting curve analysis to establish HLA genotypic identity. Tissue Antigens 2004;64:156–64.
5. Herrmann MG, Durtschi JD, Bromley LK, Wittwer CT, Voelkerding KV. Amplicon DNA melting analysis for mutation scanning and genotyping: cross-platform comparison of instruments and dyes. Clin Chem 2006;52: 494–503.
6. Herrmann MG, Durtschi JD, Bromley LK, Wittwer CT, Voelkerding KV. Instrument comparison for heterozygote scanning of single and double heterozygotes: a correction and extension of Herrmann et al. Clin Chem 2006;52:494–503. Clin Chem 2007;53:150–2.
7. Liew M, Pryor R, Palais R, Meadows C, Erali M, Lyon E, et al. Genotyping of single-nucleotide polymorphisms by high-resolution melting of small amplicons. Clin Chem 2004;50:1156–64.
8. Graham R, Liew M, Meadows C, Lyon E, Wittwer CT. Distinguishing different DNA heterozygotes by high-resolution melting. Clin Chem 2005;51:1295–8.
9. Gundry CN, Vandersteen JG, Reed GH, Pryor RJ, Chen J, Wittwer CT. Amplicon melting analysis with labeled primers: a closed-tube method for differentiating homozygotes and heterozygotes. Clin Chem 2003;49:396–406.
10. Palais RA, Liew MA, Wittwer CT. Quantitative heteroduplex analysis for single nucleotide polymorphism genotyping. Anal Biochem 2005;346:167–75.
11. Wittwer CT, Reed GH, Gundry CN, Vandersteen JG, Pryor RJ. High-resolution genotyping by amplicon melting analysis using LCGreen. Clin Chem 2003; 49:853–60.
12. Zhou L, Wang L, Palais R, Pryor R, Wittwer CT. High-resolution DNA melting analysis for simultaneous mutation scanning and genotyping in solution. Clin Chem 2005;51:1770–7.
13. Liew M, Seipp M, Durtschi J, Margraf RL, Dames S, Erali M, et al. Closed-tube SNP genotyping without labeled probes/a comparison between unlabeled probe and amplicon melting. Am J Clin Pathol 2007;127:1–8.
14. Nellaker C, Wallgren U, Karlsson H. Molecular beacon-based temperature control and automated analyses for improved resolution of melting temperature analysis using SYBR I Green chemistry. Clin Chem 2007;53:98–103.
15. Seipp M, Durtschi J, Liew M, Williams J, Damjanovich K, Pont-Kingdon G, et al. Unlabled oligonucleotides as internal temperature controls for genotyping by amplicon melting. J Mol Diagn 2007;9:284–9.

DOI: 10.1373/clinchem.2007.088120

Cell Metabolism

Adiponectin Stimulates AMP-Activated Protein Kinase in the Hypothalamus and Increases Food Intake

Naoto Kubota,[1,2,3] Wataru Yano,[1,15] Tetsuya Kubota,[1,3,4,15] Toshimasa Yamauchi,[1,2] Shinsuke Itoh,[1] Hiroki Kumagai,[1] Hideki Kozono,[1] Iseki Takamoto,[1,2,3] Shiki Okamoto,[5] Tetsuya Shiuchi,[5] Ryo Suzuki,[1,2] Hidemi Satoh,[1] Atsushi Tsuchida,[1] Masao Moroi,[4] Kaoru Sugi,[4] Tetsuo Noda,[6,7] Hiroyuki Ebinuma,[8] Yoichi Ueta,[9] Tatsuya Kondo,[10] Eiichi Araki,[10] Osamu Ezaki,[11] Ryozo Nagai,[12,13] Kazuyuki Tobe,[1,2] Yasuo Terauchi,[14] Kohjiro Ueki,[1,13] Yasuhiko Minokoshi,[5] and Takashi Kadowaki[1,2,3,*]

[1] Department of Metabolic Diseases, Graduate School of Medicine, University of Tokyo, 7-3-1 Hongo, Bunkyo-ku, Tokyo 113-8655, Japan

[2] CREST, Japan Science and Technology Corporation, 4-1-8 Honcho, Kawaguchi, Saitama 332-0012, Japan

[3] Clinical Nutrition Program, National Institute of Health and Nutrition, 1-23-1 Toyama, Shinjuku-ku, Tokyo 162-8636, Japan

[4] Division of Cardiovascular Medicine, Toho University, Ohashi Hospital, 2-17-6 Ohashi, Meguro-ku, Tokyo 153-8515, Japan

[5] Division of Endocrinology and Metabolism, National Institute for Physiological Sciences, 38 Nishigonaka, Myodaiji, Okazaki 444-8585, Japan

[6] Department of Cell Biology, Cancer Institute, Japanese Foundation for Cancer Research, 3-10-6 Ariake, Koto-ku, Tokyo 135-8550, Japan

[7] Department of Molecular Genetics, Tohoku University School of Medicine, 2-1 Seiryo-cho, Aoba-ku, Sendai, Miyagi 980-8575, Japan

[8] Diagnostics Research Laboratories, Daiichi Pure Chemicals, 3-3-1 Koyodai, Ryugasaki, Ibaraki 301-0852, Japan

[9] Department of Physiology, School of Medicine, University of Occupational and Environmental Health, 1-1 Iseigaoka, Yahata-nishi-ku, Kitakyushu, Fukuoka 807-8555, Japan

[10] Department of Metabolic Medicine, Graduate School of Medical Sciences, Kumamoto University, 1-1-1 Honjo, Kumamoto, Kumamoto 860-8556, Japan

[11] Nutritional Science Program, National Institute of Health and Nutrition, 1-23-1 Toyama, Shinjuku-ku, Tokyo 162-8636, Japan

[12] Department of Cardiovascular Diseases, Graduate School of Medicine, University of Tokyo, 7-3-1 Hongo, Bunkyo-ku, Tokyo 113-8655, Japan

[13] The 21st Century Center of Excellence Program, University of Tokyo, 7-3-1 Hongo, Bunkyo-ku, Tokyo 113-8655, Japan

[14] Department of Diabetes and Endocrinology, Yokohama City University School of Medicine, 3-9 Fukuura, Kanazawa-ku, Yokohama, Kanagawa 236-0004, Japan

[15] These authors contributed equally to this work.

*Correspondence: kadowaki-3im@h.u-tokyo.ac.jp

DOI 10.1016/j.cmet.2007.06.003

SUMMARY

Adiponectin has been shown to stimulate fatty acid oxidation and enhance insulin sensitivity through the activation of AMP-activated protein kinase (AMPK) in the peripheral tissues. The effects of adiponectin in the central nervous system, however, are still poorly understood. Here, we show that adiponectin enhances AMPK activity in the arcuate hypothalamus (ARH) via its receptor AdipoR1 to stimulate food intake; this stimulation of food intake by adiponectin was attenuated by dominant-negative AMPK expression in the ARH. Moreover, adiponectin also decreased energy expenditure. Adiponectin-deficient mice showed decreased AMPK phosphorylation in the ARH, decreased food intake, and increased energy expenditure, exhibiting resistance to high-fat-diet-induced obesity. Serum and cerebrospinal fluid levels of adiponectin and expression of AdipoR1 in the ARH were increased during fasting and decreased after refeeding. We conclude that adiponectin stimulates food intake and decreases energy expenditure during fasting through its effects in the central nervous system.

INTRODUCTION

White adipose tissue (WAT) is a major site of energy storage and plays an important role in energy homeostasis. It is also recognized as an important endocrine organ that secretes a number of biologically active adipokines (Kahn, 2000). Adiponectin, an adipokine secreted exclusively by the WAT, is present at relatively high concentrations in the circulation (Kadowaki, et al., 2006; Scherer, 2006). Adiponectin has been shown to increase the sensitivity of peripheral tissues to insulin, and it has been suggested that the decreased circulating levels of adiponectin in obesity and type 2 diabetes may contribute to the insulin resistance that characterizes both conditions (Berg et al., 2001; Fruebis et al., 2001; Yamauchi et al., 2001; Kadowaki, et al., 2006; Scherer, 2006). In humans, plasma

adiponectin levels have been shown to be negatively correlated with the body weight, body fat mass, and degree of insulin resistance, and weight reduction in obese individuals has been shown to be accompanied by an increase in plasma adiponectin concentrations (Kadowaki, et al., 2006; Scherer, 2006). Administration of recombinant adiponectin to rodents increases glucose uptake and fat oxidation in muscle, reduces hepatic glucose production, and improves whole-body insulin sensitivity (Berg et al., 2001; Fruebis et al., 2001; Yamauchi et al., 2001). Adiponectin-deficient (*adipo*$^{-/-}$) mice exhibit insulin resistance and glucose intolerance (Kubota et al., 2002; Nawrocki et al., 2006).

Adiponectin structurally belongs to the collagen superfamily and shares homologies with the collagens, complement factors, and TNFα (Scherer et al., 1995). Monomeric subunits oligomerize to form trimers that further associate through disulfide bonds within the collagenous domain to form hexamers and the high-molecular-weight (HMW) 12- to 18-mers (Pajvani et al., 2003). The HMW multimers are present in abundance in human serum and are thought to be among the more active forms of the protein (Kadowaki, et al., 2006; Scherer, 2006).

AMP-activated protein kinase (AMPK) plays a key role in the regulation of energy homeostasis (Hardie, 2004; Carling, 2005; Luo, et al., 2005) and has recently been found to mediate the stimulation of fatty acid oxidation induced by leptin (Minokoshi et al., 2002) and adiponectin (Yamauchi et al., 2002) in skeletal muscle. Remarkably, AMPK also appears to be closely involved in energy homeostasis in the central nervous system (CNS) (Hardie, 2004; Carling, 2005; Kim and Lee, 2005). Decrease in AMPK activity in the hypothalamus has been suggested to lead to reduced food intake and increased energy expenditure (Hardie, 2004; Carling, 2005; Kim and Lee, 2005). Suppression of AMPK activity seems to mediate the decrease in food intake induced by leptin because expression of active mutants of AMPK and dominant-negative inhibitory mutants of AMPK in the hypothalamus stimulate and inhibit food intake, respectively (Minokoshi et al., 2004).

In addition to its peripheral actions on the liver and skeletal muscle, including activation of AMPK and enhancement of whole-body insulin sensitivity, adiponectin has also been reported to have central actions (Qi et al., 2004). Adiponectin increases oxygen consumption and thermogenesis, which lead to weight loss, and the degree of weight loss is similar to that induced by leptin in C57BL/6 or *ob/ob* mice, despite having no effect on food intake (Qi et al., 2004). Recently, however, it was reported that adiponectin is undetectable in human cerebrospinal fluid (CSF) and that it does not cross the blood-brain barrier (BBB), although both isoforms of the adiponectin receptor, AdipoR1 and AdipoR2 (Yamauchi et al., 2003), have been demonstrated to be expressed in brain endothelial cells (Spranger et al., 2006). Thus, the physiological role of adiponectin in the CNS remains controversial.

In this study, we demonstrate the presence of adiponectin in the CSF and also show that adiponectin enters the CSF from the circulation; interestingly, only trimers and hexamers were found, and unlike in the serum, HMW multimers could not be detected in the CSF. In addition, we show that adiponectin enhances AMPK activity in the arcuate hypothalamus (ARH) via its receptor AdipoR1 and stimulates food intake, and also that this stimulation of food intake by adiponectin is attenuated by dominant-negative AMPK expression in the ARH. Moreover, adiponectin also decreases the energy consumption. Consistent with these findings, *adipo*$^{-/-}$ mice showed decreased AMPK phosphorylation in the ARH. These mice also showed reduced food intake and increased energy expenditure, thereby exhibiting resistance to high-fat diet (HFD)-induced obesity. Taken together, these findings indicate a physiological role of adiponectin in the regulation of food intake via regulation of AMPK activity in the ARH.

RESULTS

Adiponectin Receptors Are Present in the Hypothalamus, and Adiponectin Enters the CSF from the Circulation

Both the major isoforms of the adiponectin receptor, AdipoR1 and AdipoR2 (Yamauchi et al., 2003), were found to be abundantly expressed in the hypothalamus, and their expression levels were comparable to those in the liver (Figure 1A). In situ hybridization analysis using antisense probes revealed expression of AdipoR1 and AdipoR2 as well as the leptin receptor in the ARH (Figure 1B), whereas no receptor expression was detected in the hypothalamus when sense probes for AdipoR1 and AdipoR2 were used (see Figure S1A in the Supplemental Data available with this article online). Expression of AdipoR1 and AdipoR2 was also confirmed in the paraventricular hypothalamus (PVH) (Figure 1C). Immunohistochemical analysis revealed colocalization of AdipoR1 and the leptin receptor in the ARH of C57BL/6 mice (Figure 1D), but not *db/db* or AdipoR1-knockout mice (Figure S1B; Yamauchi et al., 2007).

Adiponectin was detected in the CSF of C57BL/6 mice at approximately 1/4000th of its concentration in the serum; it was also detected in the CSF of *adipo*$^{-/-}$ mice (Kubota et al., 2002; Kubota et al., 2006) 3 hr after intravenous (i.v.) injection of full-length adiponectin (1 mg/kg) administered to raise the serum adiponectin levels in these mice to approximately the same levels as in wild-type mice (Figure 1E). These findings indicate that adiponectin does indeed enter the CSF from the circulation. Adiponectin is known to exist in three forms, namely, trimers, hexamers, and HMW multimers, in the serum of wild-type mice (Figure 1F, left panel). Interestingly, unlike in the serum, only trimers and hexamers, and not HMW multimers, were found in the CSF of the wild-type mice (Figure 1F, right panel). In *adipo*$^{-/-}$ mice, at 3 hr after i.v. injection of full-length adiponectin (1 mg/kg), all three forms, i.e., trimers, hexamers, and HMW multimers, were found in the serum (Figure 1G, left panel), while only trimers and hexamers, and not HMW multimers, were found in the CSF (Figure 1G, right panel). These data indicate that the distribution of the multimeric forms of adiponectin in the CSF differs from that in the serum. It should also be noted

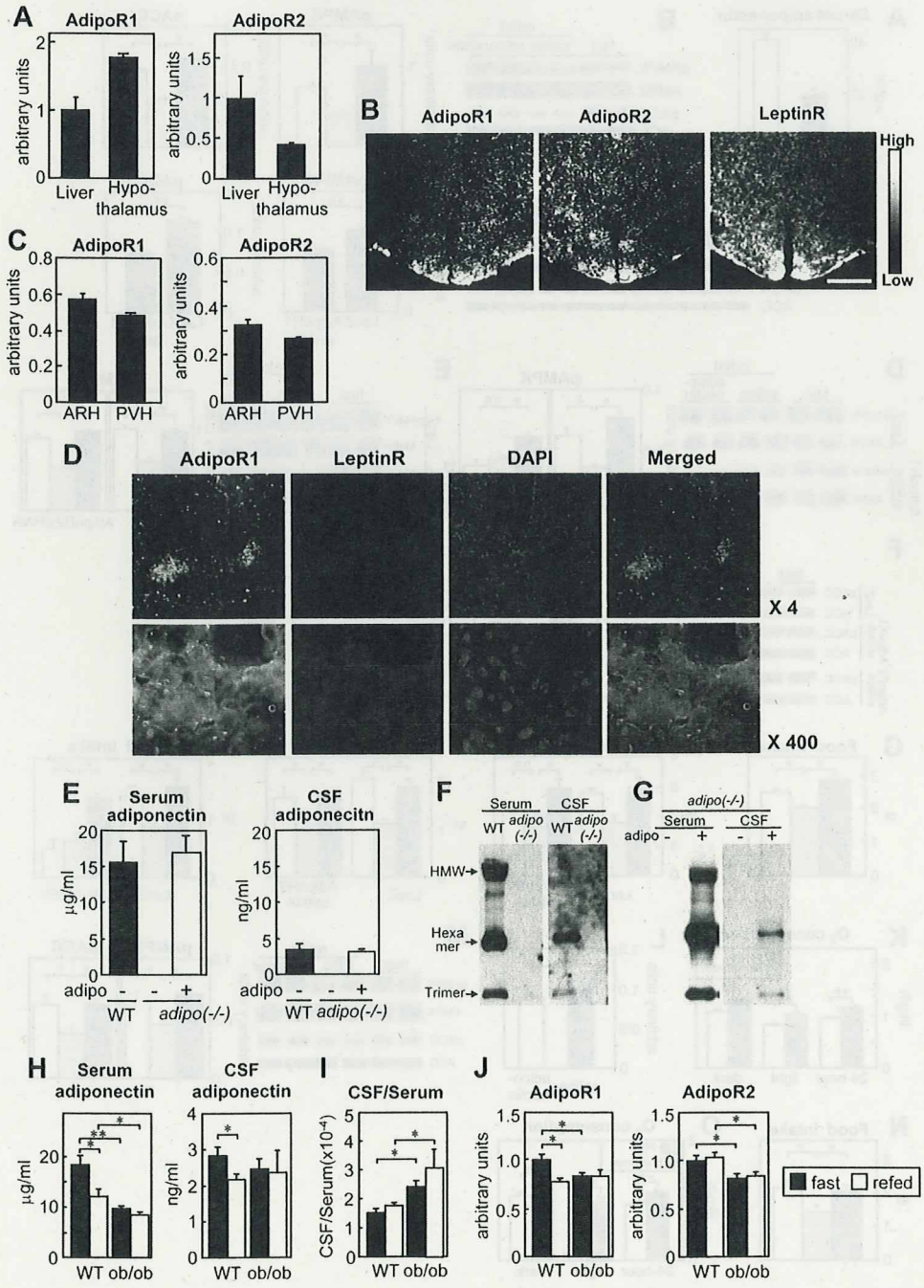

Figure 1. Adiponectin Receptors Are Present in the Hypothalamus, and Adiponectin Enters the CSF from the Circulation

(A) AdipoR1 and AdipoR2 expression levels in the hypothalamus and liver in C57BL/6 mice (n = 5). In this and all other figures, error bars represent ±SEM.

(B) In situ hybridization for AdipoR1, AdipoR2, and the leptin receptor in brain sections of C57BL/6 mice containing hypothalamic tissue (n = 3). Scale bar = 1 mm.

(C) AdipoR1 and AdipoR2 expression levels in the arcuate hypothalamus (ARH) and paraventricular hypothalamus (PVH) in C57BL/6 mice (n = 6).

(D) Immunohistochemistry for AdipoR1 and the leptin receptor in the hypothalamus of C57BL/6 mice. Magnification ×4 (upper panels); ×400 (lower panels).

(E) Adiponectin concentration in the serum and CSF of C57BL/6 mice and *adipo*$^{-/-}$ mice at 3 hr after intravenous (i.v.) injection of full-length adiponectin (1 mg/kg) (n = 4).

(F and G) Multimeric forms of adiponectin in the serum and CSF of C57BL/6 and *adipo*$^{-/-}$ mice (F) and *adipo*$^{-/-}$ mice at 3 hr after i.v. injection of full-length adiponectin (1 mg/kg) (G) (n = 3) as determined by SDS-PAGE under nonreducing and non-heat-denaturing conditions.

(H–J) Adiponectin concentrations in the serum and CSF (H), CSF-to-serum adiponectin ratios (I), and AdiopoR1 and AdipoR2 expression levels in the ARH (J) in C57BL/6 and *ob/ob* mice after 12 hr fasting followed by 3 hr refeeding (n = 8–11).

All experiments illustrated in this figure were performed using 11- to 13-week-old male mice. *$p < 0.05$; **$p < 0.01$.

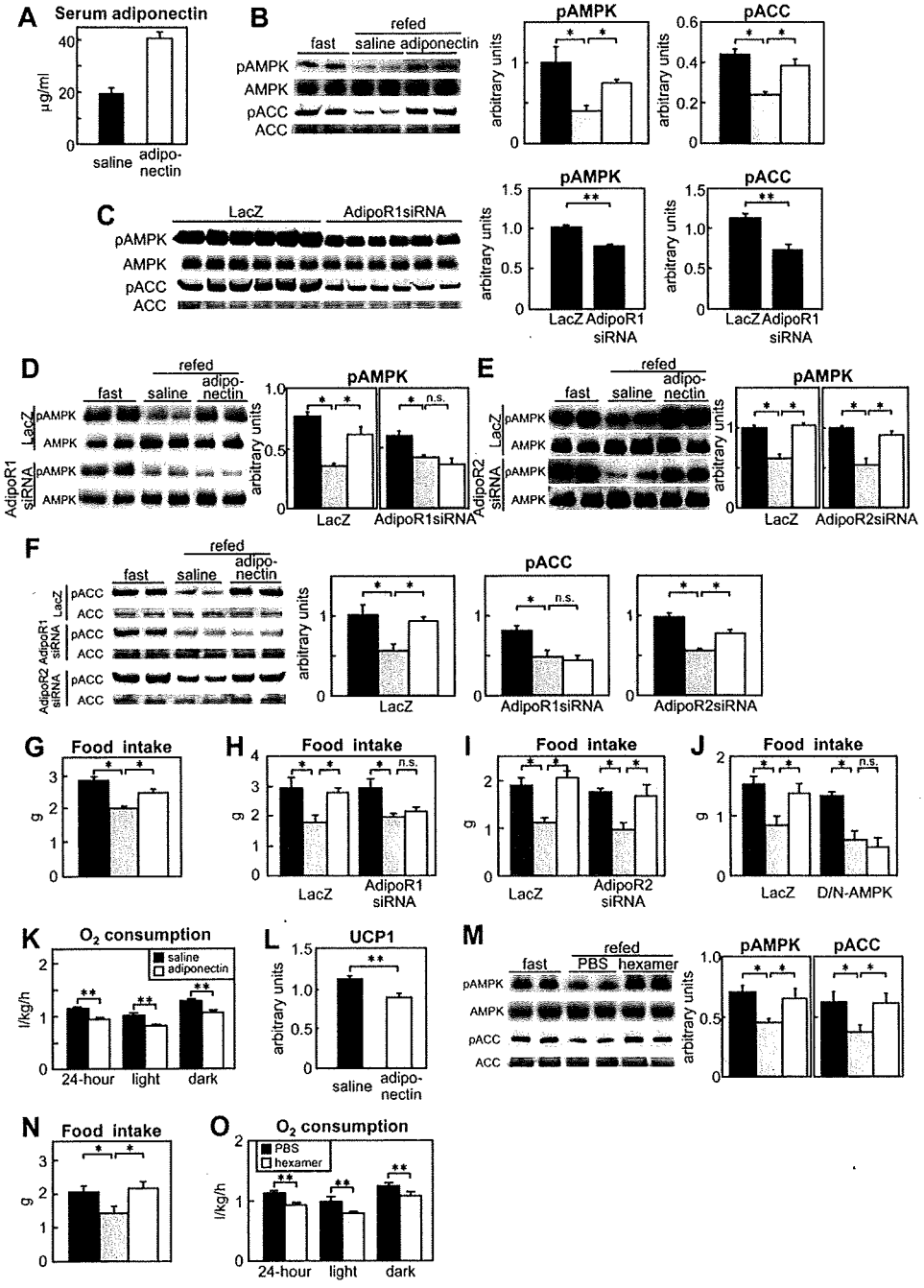

Figure 2. Adiponectin Increases AMPK Activity in the ARH and Food Intake via AdipoR1

(A) Serum adiponectin levels at 3 hr after i.v. injection of saline or full-length adiponectin (1 mg/kg) in C57BL/6 mice (n = 5).

(B–F) These experiments were performed according to protocol 1 (Figure S3A). Black bars indicate AMPK and ACC phosphorylation in group 1, gray bars indicate AMPK and ACC phosphorylation in group 2 administered an i.v. injection of saline, and white bars indicate AMPK and ACC phosphorylation in group 3 administered an i.v. injection of full-length adiponectin (1 mg/kg) (n = 6).

(B) AMPK and ACC phosphorylation in the ARH of C57BL/6 mice.

(C) AMPK and ACC phosphorylation in the ARH of C57BL/6 mice injected with adeno-LacZ or adeno-AdipoR1 siRNA under fasting conditions.

(D) AMPK phosphorylation in the ARH of C57BL/6 mice injected with adeno-LacZ or adeno-AdipoR1 siRNA.

(E) AMPK phosphorylation in the ARH of C57BL/6 mice injected with adeno-LacZ or adeno-AdipoR2 siRNA.

(F) ACC phosphorylation in the ARH of C57BL/6 mice injected with adeno-LacZ, adeno-AdipoR1 siRNA, or adeno-AdipoR2 siRNA.

(G–J) Food intake was measured according to protocol 2 (Figure S3B). Black bars indicate food intake by group 1, gray bars indicate food intake by group 2 administered an i.v. injection of saline, and white bars indicate food intake by group 3 administered an i.v. injection of full-length adiponectin (1 mg/kg) (n = 6).

that the multimeric forms of intravenously injected adiponectin found in the CSF (Figure 1G, right panel) were the same as those of the endogenous adiponectin found in the CSF of wild-type mice (Figure 1F, right panel).

Serum adiponectin levels in *ob/ob* mice were significantly lower than those in wild-type mice, both under fasting conditions and after refeeding (Figure 1H, left panel). In wild-type mice, while plasma levels of glucose and insulin and serum levels of leptin increased significantly after refeeding (Figures S2A–S2C), serum adiponectin levels decreased significantly (Figure 1H, left panel). In contrast, in *ob/ob* mice, serum adiponectin levels remained unchanged even after refeeding (Figure 1H, left panel). Unlike in the serum, CSF adiponectin levels in *ob/ob* mice were similar to those in wild-type mice both under fasting conditions and after refeeding (Figure 1H, right panel). However, while CSF adiponectin levels decreased significantly after refeeding in wild-type mice (Figure 1H, right panel), the levels in *ob/ob* mice remained unaltered even after refeeding (Figure 1H, right panel). In addition, the ratios of CSF to serum adiponectin levels were significantly higher in *ob/ob* mice than those in wild-type mice both under fasting conditions and after refeeding (Figure 1I). These findings indicate that, unlike serum adiponectin levels, CSF adiponectin levels, which were relatively higher in *ob/ob* mice, may not be correlated with obesity or obesity-linked insulin resistance. In wild-type mice, the expression of AdipoR1 in the ARH decreased significantly after refeeding, whereas that of AdipoR2 remained unchanged (Figure 1J). On the other hand, the expression of both AdipoR1 and AdipoR2 remained unchanged after refeeding in *ob/ob* mice (Figure 1J).

Adiponectin Increases AMPK Activity in the ARH via AdipoR1 to Stimulate Food Intake

In view of the increases in adiponectin concentrations in the serum and CSF and the increases in the AdipoR1 expression level in the ARH under fasting conditions, adiponectin signals may be involved in the stimulation of food intake. It has been suggested that adiponectin is an orexigenic hormone and that it may stimulate the phosphorylation of AMPK and acetyl-CoA carboxylase (ACC), downstream of AMPK, in the hypothalamus (Hardie, 2004; Andersson et al., 2004; Carling, 2005; Xue and Kahn, 2006). To evaluate this effect of adiponectin, wild-type mice were divided into three groups, as follows, after 12 hr fasting during the dark phase of the light/dark cycle (Figure S3A, protocol 1): group 1, in which the ARH was sampled immediately; group 2, in which the mice were allowed access to food for the first 3 hr and then administered an i.v. infusion of saline for 3 hr prior to ARH sampling; and group 3, in which the mice were allowed access to food for the first 3 hr and then administered an i.v. injection of adiponectin, followed 3 hr later by ARH sampling. Serum adiponectin levels were 2-fold higher 3 hr after adiponectin injection in group 3 than after saline injection in group 2 (Figure 2A). Phosphorylation of AMPK and ACC was suppressed after refeeding (Figure 2B) (Andersson et al., 2004; Minokoshi et al., 2004; Xue and Kahn, 2006). Administration of adiponectin increased the phosphorylation of threonine 172, which is known to stimulate AMPK activity (Hardie, 2004; Carling, 2005), of AMPK in group 3 (Figure 2B). Consistent with this, adiponectin also increased the phosphorylation of ACC (Figure 2B), which is a downstream target of AMPK, although the possible effect of other signaling pathways on ACC phosphorylation cannot be entirely excluded.

Next, we investigated whether the enhanced AMPK activation by adiponectin was mediated by the adiponectin receptors expressed in the ARH by injecting adeno-AdipoR1 siRNA or adeno-AdipoR2 siRNA into the ARH, using adeno-LacZ as a control. We confirmed that the adenovirus vectors had been successfully injected into the ARH by the observation of positive LacZ immunostaining in the region (Figure S4A). The phosphorylation of AMPK and ACC in the ARH was significantly suppressed in the adeno-AdipoR1 siRNA-treated mice as compared with the adeno-LacZ-treated mice under fasting conditions (Figure 2C). After refeeding, phosphorylation of AMPK and ACC was also suppressed in the control group treated with adeno-LacZ, and this was reversed by the administration of adiponectin (Figures 2D and 2F). However, in the animals in which AdipoR1 expression in the ARH was decreased by treatment with AdipoR1 siRNA (Figures S4B and S4C), adiponectin failed to reverse the suppression of AMPK and ACC phosphorylation observed after refeeding (Figures 2D and 2F). On the other hand, when AdipoR2 expression in the ARH was reduced by the administration of AdipoR2 siRNA (Figure S4D), the suppression of AMPK and ACC phosphorylation after refeeding was still

(G) Food intake by C57BL/6 mice.
(H) Adeno-LacZ or adeno-AdipoR1 siRNA was injected into the ARH of C57BL/6 mice.
(I) Adeno-LacZ or adeno-AdipoR2 siRNA was injected into the ARH of C57BL/6 mice.
(J) Adeno-LacZ or adeno-D/N-AMPK was injected into the ARH of C57BL/6 mice.
(K) Oxygen consumption in fasting C57BL/6 mice injected i.v. with saline or adiponectin (1 mg/kg) (n = 7).
(L) UCP1 expression in brown adipose tissue (BAT) after 12 hr fasting (n = 4–5).
(M) This experiment was performed according to protocol 1 (Figure S3A). Black bars indicate AMPK and ACC phosphorylation in group 1, gray bars indicate AMPK and ACC phosphorylation in group 2 administered an intracerebroventricular (i.c.v.) injection of PBS, and white bars indicate AMPK and ACC phosphorylation in group 3 administered an i.c.v. injection of the hexameric form of adiponectin (150 ng) (n = 6).
(N) Food intake was measured according to protocol 2 (Figure S3B). Black bar indicates food intake by group 1, gray bar indicates food intake by group 2 administered an i.c.v. injection of PBS, and white bar indicates food intake by group 3 administered an i.c.v. injection of the hexameric form of adiponectin (150 ng) (n = 8).
(O) Oxygen consumption in fasting C57BL/6 mice administered an i.c.v. injection of the hexameric form of adiponectin (150 ng) (n = 7).
All experiments illustrated in this figure were performed using 11- to 13-week-old male mice. *$p < 0.05$; **$p < 0.01$.

reversed by adiponectin (Figures 2E and 2F). These findings suggest that adiponectin directly activates AMPK in the ARH via AdipoR1, but not AdipoR2.

Since increased AMPK activity in the ARH has been shown to stimulate food intake (Hardie, 2004; Minokoshi et al., 2004; Carling, 2005), we then investigated the effect of adiponectin on food intake. In accordance with the protocol used to measure the AMPK activity, wild-type mice were divided into three groups, as follows, after 12 hr fasting during the dark phase of the light/dark cycle, and the amount of food intake was measured over a period of 6 hr (Figure S3B, protocol 2): group 1, in which the mice were immediately allowed access to food throughout the 6 hr; group 2, in which the mice were allowed access to food for 3 hr and then administered an i.v. infusion of saline, and food intake was measured over the next 6 hr; and group 3, in which the mice were allowed access to food for 3 hr and then administered an i.v. injection of adiponectin, and food intake was measured over the next 6 hr. Food intake after refeeding (group 2) (Figure 2G, gray bar) was significantly lower than after fasting (group 1) (Figure 2G, black bar), as the AMPK and ACC phosphorylation levels decreased (Figure 2B). Adiponectin injection significantly increased food intake after refeeding (group 3) (Figure 2G, white bar), as the AMPK and ACC phosphorylation levels increased (Figure 2B). In the mice in which AdipoR1 expression in the ARH was decreased by treatment with AdipoR1 siRNA (Figures S4B and S4C), the stimulation of food intake by adiponectin injection (Figure 2H, left, white bar) was blunted (Figure 2H, right, white bar). On the other hand, in the mice in which AdipoR2 expression in the ARH was decreased by treatment with AdipoR2 siRNA (Figure S4D), no such blunting of the effect of adiponectin injection was observed (Figure 2I, right, white bar). These findings suggest that adiponectin stimulates food intake via AdipoR1 in the ARH.

Next, in order to investigate whether the stimulation of food intake induced by adiponectin is actually mediated by AMPK, dominant-negative AMPK (D/N-AMPK) was expressed in the ARH, and the amount of food intake over a period of 6 hr was measured according to protocol 2 described above (Figure S3B). In the control group treated with LacZ, the amount of food consumed after adiponectin injection (group 3) (Figure 2J, left, white bar) was significantly higher than after saline injection (group 2) (Figure 2J, left, gray bar). In contrast, in the group treated with D/N-AMPK, the stimulation of food intake by the adiponectin injection (Figure 2J, left, white bar) was blunted (Figure 2J, right, white bar), suggesting that adiponectin has a central action of stimulating food intake by activating AMPK in the ARH. In addition to regulating food intake, AMPK in the hypothalamus is also thought to regulate energy expenditure (Hardie, 2004; Carling, 2005; Kim and Lee, 2005). Examination of the effect of adiponectin on energy expenditure revealed that oxygen consumption during the light and dark phases of the 24 hr cycle was significantly decreased by adiponectin (Figure 2K). Consistent with these findings, expression of uncoupling protein 1 (UCP1) in brown adipose tissue (BAT) was significantly decreased at 12 hr after i.v. injection of adiponectin (Figure 2L).

We then administered the hexameric form of adiponectin (Figure S4E), the predominant form in the CSF (Figure 1F), directly into the lateral cerebral ventricles and examined the direct effects of adiponectin in order to rule out the possibility that the actions of adiponectin on the peripheral organs participate in the AMPK activation in the ARH and stimulation of food intake. The suppression of AMPK and ACC phosphorylation after refeeding was indeed reversed by intracerebroventricular (i.c.v.) administration of the hexameric form of adiponectin (Figure S3A, protocol 1) (Figure 2M). i.c.v. injection of the hexameric form of adiponectin also significantly stimulated food intake after refeeding (Figure S3B, protocol 2) (Figure 2N, white bar), along with increasing the AMPK and ACC phosphorylation levels (Figure 2M). Moreover, oxygen consumption during the light and dark phases of the 24 hr cycle was significantly decreased following i.c.v. injection of the hexameric form of adiponectin (Figure 2O). i.v. injection of adiponectin decreased energy expenditure (Figure 2K) and UCP1 expression in BAT (Figure 2L). Since i.c.v. injection of the hexameric form of adiponectin also decreased energy expenditure (Figure 2O), determination of UCP1 expression in BAT following i.c.v. administration may aid our understanding of the effect of adiponectin in the CNS. Taken together, these findings indicate that adiponectin directly regulates AMPK activity in the ARH and food intake.

Adiponectin Reverses Leptin-Induced Suppression of AMPK Activity in the ARH and Food Intake via AdipoR1

Because leptin has been reported to inhibit AMPK activity in the ARH and to thereby suppress food intake (Minokoshi et al., 2004), we investigated the effect of adiponectin on the leptin-induced suppression of AMPK activity in the ARH and food intake. Wild-type mice were divided into three groups, as follows, after 12 hr fasting during the dark phase of the light/dark cycle (Figure S3C, protocol 3): group 1, in which the ARH was sampled 3 hr after an i.v. injection of saline; group 2, in which the ARH was sampled 3 hr after an i.v. injection of leptin; and group 3, in which the ARH was sampled 3 hr after an i.v. injection of leptin + adiponectin. The AMPK and ACC phosphorylation in the ARH was significantly suppressed following leptin administration (group 2) (Figure 3A) (Minokoshi et al., 2004; Xue and Kahn, 2006), but the leptin-induced suppression was reversed by adiponectin (group 3) (Figure 3A). We then investigated whether the increase in AMPK activity induced by adiponectin was mediated by AdipoR1 in the ARH. The AMPK and ACC phosphorylation in the ARH of the adeno-AdipoR1 siRNA-treated mice was significantly suppressed as compared with the LacZ-treated mice under fasting conditions (Figure 3B), as shown in Figure 2C. In the control group treated with LacZ, AMPK and ACC phosphorylation was suppressed by leptin, which was again reversed by adiponectin (Figures 3C and 3D). When AdipoR1 expression in the ARH was reduced by injection of AdipoR1

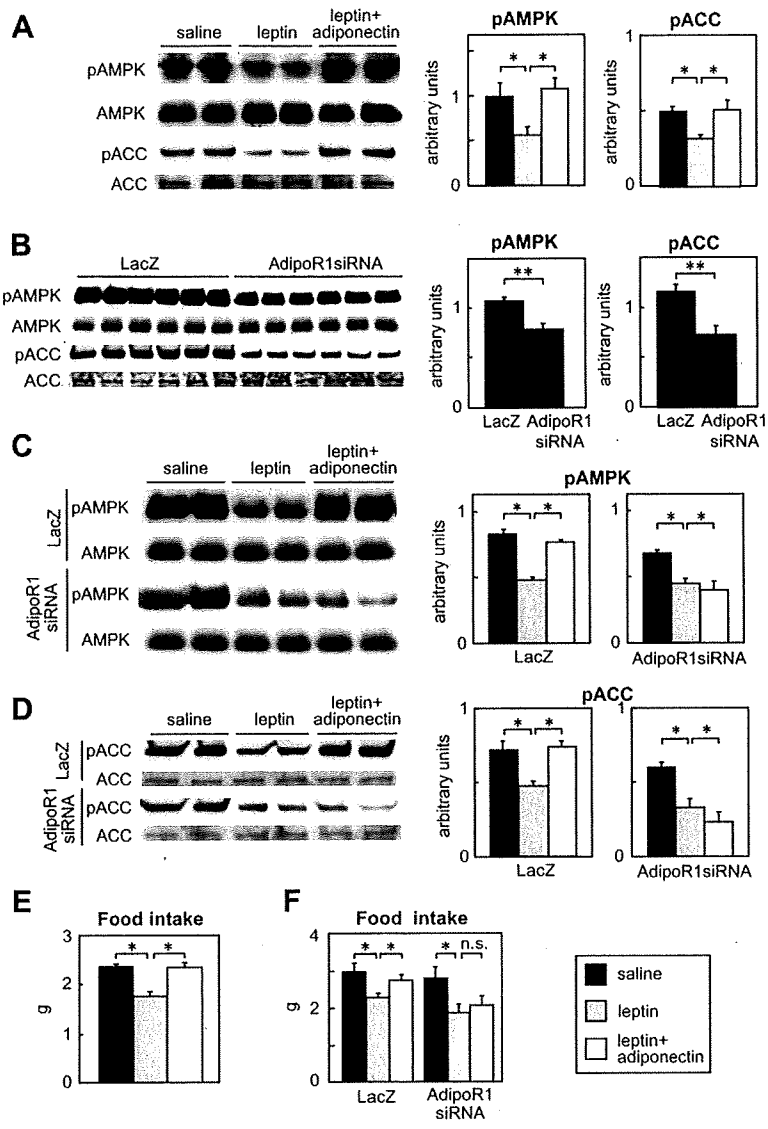

Figure 3. Adiponectin Reverses Leptin-Induced Suppression of AMPK Activity in the ARH and Food Intake via AdipoR1

(A–D) These experiments were performed according to protocol 3 (Figure S3C). Black bars indicate AMPK and ACC phosphorylation in group 1, gray bars indicate AMPK and ACC phosphorylation in group 2 administered an i.v. injection of saline, and white bars indicate AMPK and ACC phosphorylation in group 3 administered an i.v. injection of full-length adiponectin (1 mg/kg) (n = 6).

(A) AMPK and ACC phosphorylation in the ARH of C57BL/6 mice.

(B) AMPK and ACC phosphorylation in the ARH of C57BL/6 mice following injection of adeno-LacZ or adeno-AdipoR1 siRNA under fasting conditions.

(C and D) AMPK (C) and ACC (D) phosphorylation in the ARH of C57BL/6 mice following injection of adeno-LacZ or adeno-AdipoR1 siRNA.

(E and F) Food intake was measured according to protocol 4 (Figure S3D). Black bars indicate food intake by group 1, gray bars indicate food intake by group 2 administered an i.v. injection of saline, and white bars indicate food intake by group 3 administered an i.v. injection of full-length adiponectin (n = 6).

(E) Food intake by C57BL/6 mice.

(F) Adeno-LacZ or adeno-AdipoR1 siRNA was injected into the ARH of C57BL/6 mice.

All experiments illustrated in this figure were performed using 11- to 13-week-old male mice. *p < 0.05.

siRNA (Figures S4B and S4C), adiponectin failed to reverse the suppression of AMPK and ACC phosphorylation induced by leptin (Figures 3C and 3D).

In accordance with the protocol used to measure the AMPK activity, wild-type mice were divided into three groups, as follows, after 12 hr fasting during the dark phase of the light/dark cycle, and food intake was measured over a period of 6 hr (Figure S3D, protocol 4): group 1, in which the mice were administered an i.v. injection of saline; group 2, in which the mice were administered an i.v. injection of leptin; and group 3, in which the mice were administered an i.v. injection of leptin + adiponectin. We found that adiponectin reversed the suppression of food intake induced by leptin (Figure 3E). In the animals in which AdipoR1 expression in the ARH was decreased by treatment with AdipoR1 siRNA (Figures S4B and S4C), adiponectin failed to reverse the leptin-induced suppression of food intake (Figure 3F). These findings suggest that adiponectin reverses the leptin-induced suppression of AMPK activity and food intake via its central effects on AdipoR1.

adipo$^{-/-}$ Mice Exhibit Decreased AMPK Activity in the ARH, Increased Oxygen Consumption, and Greater Loss of Fat during Fasting

In order to further elucidate the physiological role of adiponectin in the CNS, we investigated the effects of adiponectin deficiency on AMPK activity, food intake, and energy homeostasis in *adipo*$^{-/-}$ mice. AMPK phosphorylation in the ARH was significantly suppressed in *adipo*$^{-/-}$ mice after 12 hr fasting (Figure 4A). Expression of neuropeptide Y (NPY) in the ARH after 12 hr fasting was also significantly lower in *adipo*$^{-/-}$ mice (Figure 4B), while the expression of pro-opiomelanocortin (POMC) in the ARH was increased after 12 hr fasting in these mice (Figure 4C). Consistent with the decreased AMPK activity and decreased NPY expression in the ARH, *adipo*$^{-/-}$ mice consumed significantly more oxygen than their wild-type littermates during the

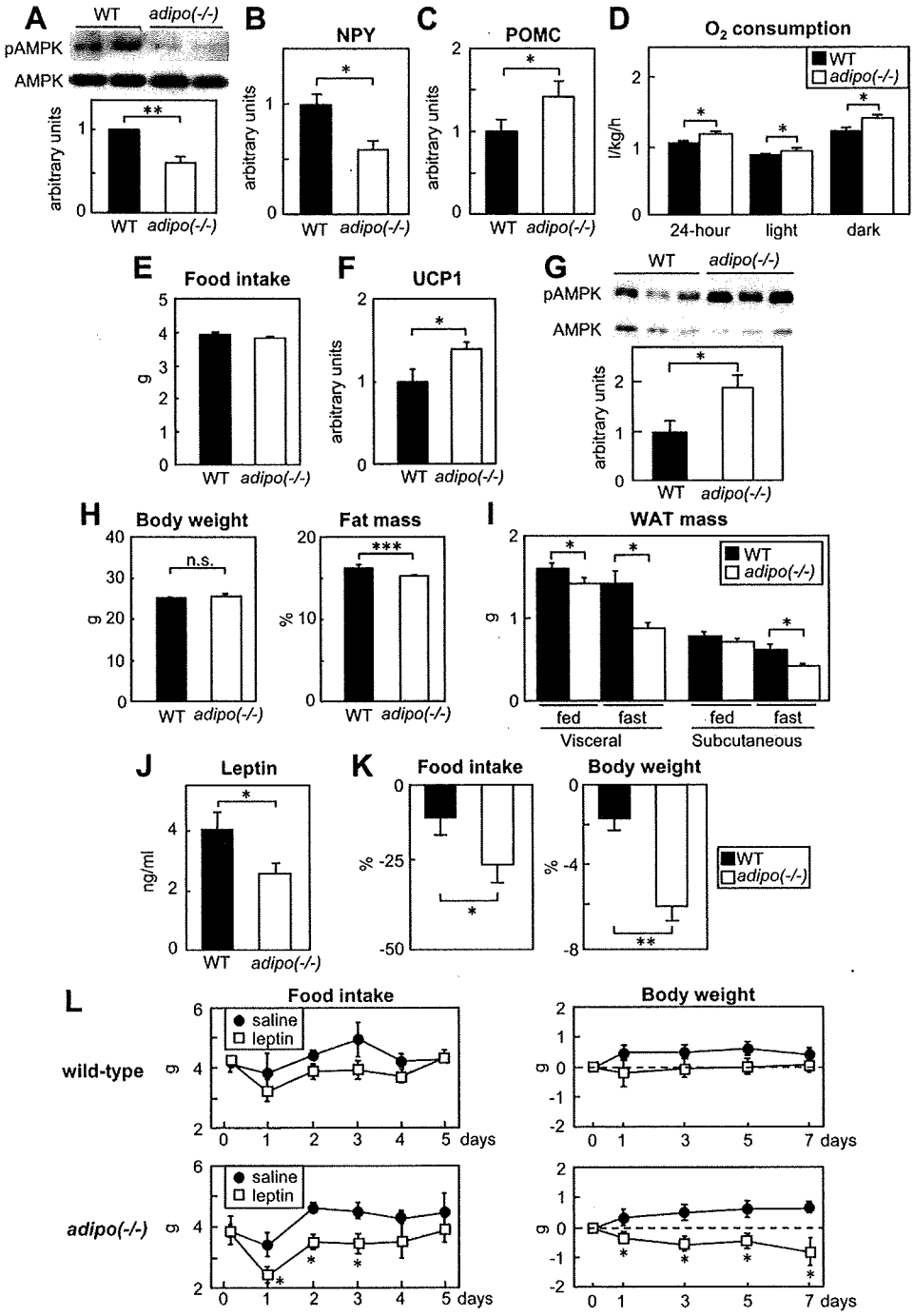

Figure 4. *adipo*$^{-/-}$ Mice Exhibit Decreased AMPK Activity in the ARH, Increased Oxygen Consumption, and Greater Loss of Fat during Fasting

(A) AMPK phosphorylation in the ARH of wild-type and *adipo*$^{-/-}$ mice after 12 hr fasting (n = 6).

(B and C) NPY (B) and POMC (C) expression in the ARH after 12 hr fasting (n = 6).

(D) Oxygen consumption in wild-type and *adipo*$^{-/-}$ mice under fasting conditions (n = 9).

(E) Daily food intake by wild-type and *adipo*$^{-/-}$ mice (n = 9–11).

(F) UCP1 expression in BAT of wild-type and *adipo*$^{-/-}$ mice (n = 6).

(G) AMPK phosphorylation in skeletal muscle of wild-type and *adipo*$^{-/-}$ mice (n = 6).

(H) Body weight (left) and fat mass measured by dual-energy X-ray absorptiometry (right) in wild-type and *adipo*$^{-/-}$ mice (n = 10–11).

(I) Visceral (epididymal, retroperitoneal, and perirenal) and subcutaneous fat mass in wild-type and *adipo*$^{-/-}$ mice before and after 12 hr fasting (n = 4–13).

(J) Serum leptin levels in wild-type and *adipo*$^{-/-}$ mice after 6 hr fasting (n = 13–15).

(K) Decreased food intake and body weight in wild-type and *adipo*$^{-/-}$ mice after intraperitoneal injection of leptin (5 mg/kg) (n = 5–7).

light and dark phases of the 24 hr cycle under fasting conditions (Figure 4D), even though food intake remained unchanged (Figure 4E). Expression of UCP1 in BAT was significantly increased in *adipo*$^{-/-}$ mice as compared with wild-type mice (Figure 4F). Moreover, despite the adiponectin deficiency, AMPK phosphorylation in skeletal muscle was significantly increased in *adipo*$^{-/-}$ mice compared to their wild-type littermates (Figure 4G). These increases in UCP1 expression and AMPK phosphorylation, which may account for the increased energy expenditure in *adipo*$^{-/-}$ mice, cannot be explained by the peripheral actions of adiponectin but may presumably be explainable by its central actions.

Despite the similar body weight of wild-type and *adipo*$^{-/-}$ mice (Figure 4H, left), body fat mass, as measured by dual-energy X-ray absorptiometry (DEXA), was significantly lower in *adipo*$^{-/-}$ mice than in wild-type mice (Figure 4H, right) ($p < 0.001$). The reduction in visceral and subcutaneous fat mass after 12 hr fasting was greater in *adipo*$^{-/-}$ mice than in wild-type mice (Figure 4I). Consistent with these findings, serum leptin levels after 6 hr fasting were significantly lower in *adipo*$^{-/-}$ mice than in wild-type mice (Figure 4J). Moreover, the suppression of food intake (Figure 4K, left) and the weight loss (Figure 4K, right) induced by intraperitoneal injection of leptin (5 mg/kg) were significantly greater in *adipo*$^{-/-}$ mice than in wild-type mice, indicating that *adipo*$^{-/-}$ mice are probably more leptin sensitive than wild-type mice. To further confirm the leptin-sensitive phenotype of *adipo*$^{-/-}$ mice, we administered leptin for a week at 0.3 μg/hr to wild-type and *adipo*$^{-/-}$ mice via a subcutaneously implanted osmotic pump. Leptin infused at this dose failed to produce any significant decrease in food intake (Figure 4L, upper left panel) or body weight (Figure 4L, upper right panel) in wild-type mice. In contrast, the same dose of leptin significantly decreased both food intake (Figure 4L, lower left panel) and body weight (Figure 4L, lower right panel) in *adipo*$^{-/-}$ mice. These data confirm the higher leptin sensitivity of *adipo*$^{-/-}$ mice as compared with wild-type mice.

adipo$^{-/-}$ Mice Exhibit Reduced Food Intake and Increased Oxygen Consumption and Appear to Be Protected from High-Fat-Diet-Induced Obesity

adipo$^{-/-}$ mice were found to be more resistant to HFD-induced obesity than wild-type mice (Figure 5A). The visceral WAT mass and subcutaneous WAT mass were both significantly smaller in *adipo*$^{-/-}$ mice fed a HFD (Figure 5B). Histological analysis of WAT and quantitation of adipocyte size in the mice revealed significantly smaller adipocytes in *adipo*$^{-/-}$ mice than in wild-type mice (Figure 5C). Additionally, after 2 weeks of HFD, when the two groups were indistinguishable by body weight, we examined serum leptin levels, AMPK and ACC phosphorylation status, AdipoR1 and AdipoR2 expression, food intake, and oxygen consumption in the two groups. Serum leptin levels after 6 hr fasting were significantly lower in *adipo*$^{-/-}$ mice than in wild-type mice (Figure 5D). AMPK and ACC phosphorylation in the ARH was significantly suppressed in *adipo*$^{-/-}$ mice after 12 hr fasting (Figure 4E), although the expression levels of AdipoR1 and AdipoR2 in the ARH were not significantly different between the two genotypes (Figure 5F). Daily food intake was significantly lower in *adipo*$^{-/-}$ mice than in wild-type mice (Figure 5G), and oxygen consumption was significantly greater (Figure 5H).

DISCUSSION

In this study, we demonstrate that adiponectin activates AMPK via AdipoR1 in the hypothalamus, leading to stimulation of food intake and decrease in energy expenditure. Consistent with these findings, *adipo*$^{-/-}$ mice fed a HFD exhibit decreased AMPK phosphorylation and NPY expression in the ARH, reduced food intake, and increased energy expenditure, thereby exhibiting resistance to HFD-induced obesity. Scherer's group (Kim et al., 2007) has generated adiponectin-transgenic *ob/ob* mice that show serum adiponectin levels 3- to 4-fold higher than *ob/ob* mice. These mice also show markedly increased body weight due to decreased energy expenditure, as manifested by lower body temperature and lower oxygen consumption, consistent with our observations that adiponectin decreases energy expenditure (Figures 2K and 2O) and UCP1 expression in BAT (Figure 2L) and that *adipo*$^{-/-}$ mice exhibit increased oxygen consumption (Figure 4D and Figure 5H). We also found that serum and CSF adiponectin levels and expression of AdipoR1 in the ARH increase during fasting and decrease after refeeding, suggesting that adiponectin acts mainly under fasting conditions. Moreover, the reduction of visceral and subcutaneous fat mass that was observed after 12 hr fasting was greater in *adipo*$^{-/-}$ mice than in wild-type mice (Figure 4I). Based on these results, we propose that adiponectin serves as a starvation hormone that facilitates efficient fat storage in WAT under fasting conditions.

The blood-CSF barrier in the choroid plexus and the BBB in the cerebral endothelium are the two major sites controlling the entry of proteins into the brain (Zlokovic et al., 2000; Schwartz and Porte, 2005). The relative contributions of these two CNS transport pathways in maintaining adiponectin homeostasis in the CNS and the access pathway of adiponectin to the hypothalamus and/or other CNS targets are unknown. Nevertheless, in this study, adiponectin was shown to be present in the CSF and to enter the CSF from the circulation (Figures 1E–1G), as described by Ahima's group (Qi et al., 2004). Furthermore, the adiponectin receptors adipoR1 and adipoR2 were found to be expressed in the hypothalamus (Figures 1A–1D) and BBB endothelial cells (Spranger et al., 2006). We speculate that an adiponectin transport system mediated by adiponectin

(L) Food intake and body weight in wild-type and *adipo*$^{-/-}$ mice implanted with a subcutaneous osmotic minipump to deliver saline or 0.3 μg/hr leptin. ($n = 6–9$).
All experiments illustrated in this figure were performed using 9- to 13-week-old male mice. *$p < 0.05$; **$p < 0.01$; ***$p < 0.001$.

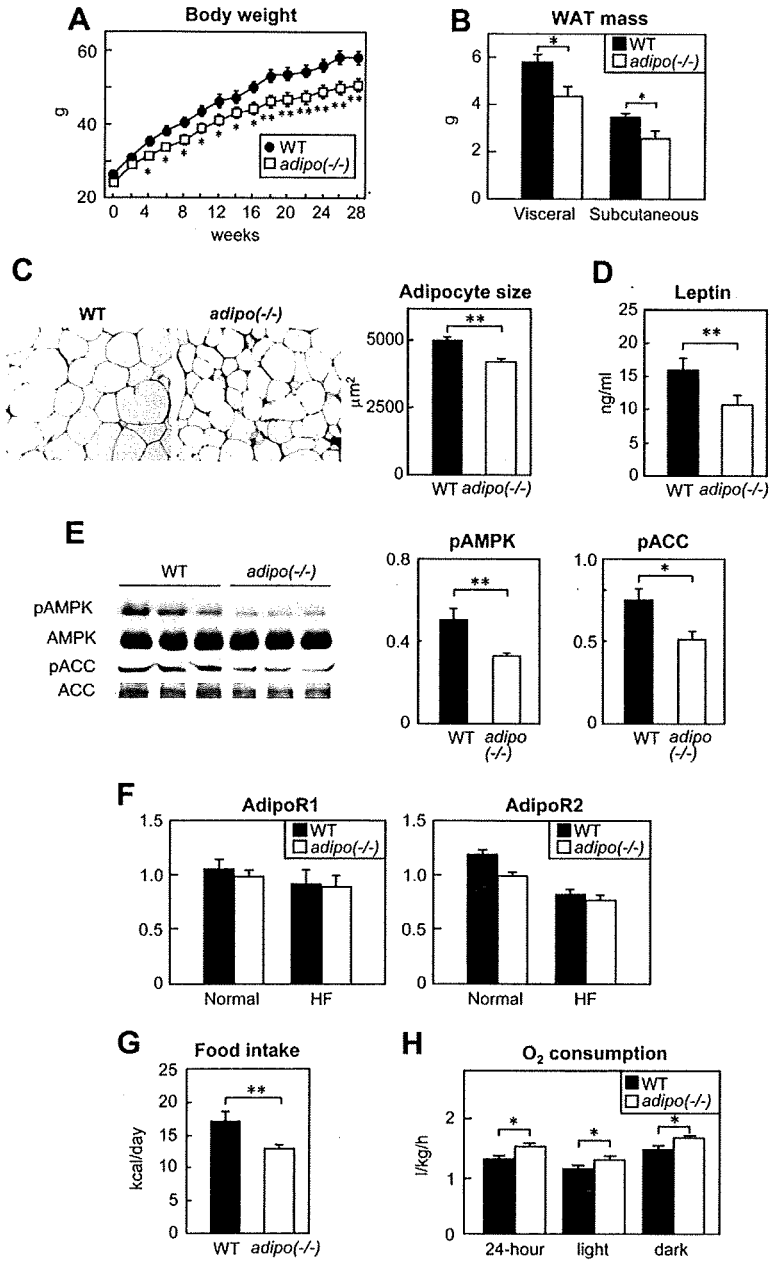

Figure 5. *adipo*$^{-/-}$ Mice Exhibit Decreased Food Intake and Increased Oxygen Consumption and Are Protected from High-Fat-Diet-Induced Obesity

(A) Body weight of wild-type and *adipo*$^{-/-}$ mice on a high-fat diet (HFD) (n = 21–24).

(B) Weight of visceral (epididymal, retroperitoneal, and perirenal) and subcutaneous fat pads after 20 weeks on HFD (n = 21–24).

(C) Histological analysis of white adipose tissue (left panels) and quantitation of adipocyte size (right panel) in wild-type and *adipo*$^{-/-}$ mice after 20 weeks on HFD (n = 7–8). Magnification ×100.

(D) Serum leptin levels after 6 hr fasting in wild-type and *adipo*$^{-/-}$ mice fed a HFD for 2 weeks (n = 6).

(E) AMPK and ACC phosphorylation after 6 hr fasting in the ARH of wild-type and *adipo*$^{-/-}$ mice fed a HFD for 2 weeks (n = 6).

(F) AdipoR1 and AdipoR2 expression levels in the ARH and PVH of wild-type and *adipo*$^{-/-}$ mice before and after administration of a HFD for 2 weeks (n = 5–8).

(G) Food intake by wild-type and *adipo*$^{-/-}$ mice after administration of a HFD for 2 weeks (n = 9).

(H) Oxygen consumption under fasting conditions in wild-type and *adipo*$^{-/-}$ mice after administration of a HFD for 2 weeks (n = 9).

*$p < 0.05$; **$p < 0.01$.

receptors in the hypothalamus and choroid plexus may regulate adiponectin entry into the CNS and CSF under physiological conditions. Further investigation is needed to verify this contention.

Although the HMW form of adiponectin is believed to be more closely associated with insulin sensitivity and is considered to be a relatively more metabolically active form than the trimeric and hexameric forms of adiponectin, it must be borne in mind that all three forms can bind to AdipoR1 and activate AMPK (Kadowaki, et al., 2006; Hada, et al., 2007). Interestingly, while the trimers, hexamers, and HMW multimers of adiponectin were found in the serum, only the trimer and hexamer forms were found in the CSF. Since HMW adiponectin consists of a large number of complexes, it may be too large to enter the CSF, which could explain the absence of HMW adiponectin in the CSF. The trimer and hexamer forms may be responsible for the central actions of adiponectin under physiological conditions. Similar to our findings, a previous study also reported finding trimers and hexamers of adiponectin, but not HMW multimers, in the human CSF (Kusminski, et al., 2007).

Why was there no effect of adiponectin deficiency on food intake in *adipo*$^{-/-}$ mice under normal diet conditions? Considering the increase in oxygen consumption observed in *adipo*$^{-/-}$ mice, one possibility is that a compensatory increase in the orexigenic pathway may contribute to the maintenance of food intake, thus preventing

these mice from experiencing excessive weight loss. On the other hand, under conditions of excess energy availability, such as in animals fed a HFD, this compensation by the increased orexigenic pathway may disappear. In fact, food intake was indeed decreased in *adipo*$^{-/-}$ mice fed a HFD (Figure 5G).

It has been reported that while adiponectin administered by i.c.v. injection induces increased oxygen consumption and weight loss, it has no effect on the food intake (Qi et al., 2004). Our data, however, indicate that i.v. injection of full-length adiponectin or i.c.v. injection of the hexameric form of adiponectin (the predominant form in the CSF) (Figure 1F) significantly stimulates food intake during refeeding (Figures 2G and 2N) and decreases oxygen consumption (Figures 2K and 2O), although body weight remained largely unchanged.

Serum levels of adiponectin have been known to be correlated inversely with obesity, insulin resistance, and diabetes; however, the *ob/ob* mice in this study failed to show any significant decrease in CSF adiponectin levels as compared with wild-type mice. In fact, the *ob/ob* mice exhibited relatively higher concentrations of adiponectin in the CSF (Figure 1I). This may indicate a lack of correlation between CSF adiponectin levels and obesity or obesity-linked insulin resistance. Recent studies have shown that adiponectin exists in human CSF at a concentration 1/1000th of that in serum (Kusminski et al., 2007; Kos et al., 2007). These data also show that there may be no association between CSF concentrations of adiponectin and obesity or insulin resistance except in obese males, which is in accordance with our findings. Thus, adiponectin may play an important role in the hypothalamus not only in mouse models but also in humans.

Based on these findings, we propose a hypothesis on the role of adiponectin in the regulation of food intake and energy homeostasis (Figure 6). Under fasting conditions, serum and CSF adiponectin levels and AdipoR1 expression in the ARH increase; consequently, hypothalamic AMPK is activated, which stimulates food intake and suppresses energy expenditure, promoting fat storage. After refeeding, on the other hand, serum and CSF adiponectin levels and AdipoR1 expression in the ARH decrease; consequently, hypothalamic AMPK activity decreases, resulting in reduced food intake and increased energy expenditure. Serum leptin levels are regulated inversely in relation to serum adiponectin levels both under fasting conditions and after refeeding. Leptin suppresses hypothalamic AMPK activity and food intake, as opposed to the action of adiponectin. Thus, central adiponectin/leptin signals may represent the physiological pathway by which hypothalamic AMPK activity and food intake are stimulated during fasting and suppressed after refeeding.

In addition to this short-term regulation of food intake and energy expenditure by adiponectin and leptin, these two adipokines may also participate in the long-term regulation of energy homeostasis. The fundamental roles of leptin and adiponectin seem to be to preserve an adequate fat reserve: leptin acts as a satiety signal, and adiponectin acts as a starvation signal. During the course of evolution, starvation signals are essential for the survival of an organism, whereas satiety signals develop later as a complementary system in periods of occasional excessive food intake and fat storage. This may explain why, unlike the leptin receptor, the adiponectin receptor homolog has been conserved from yeast to humans (Karpichev et al., 2002).

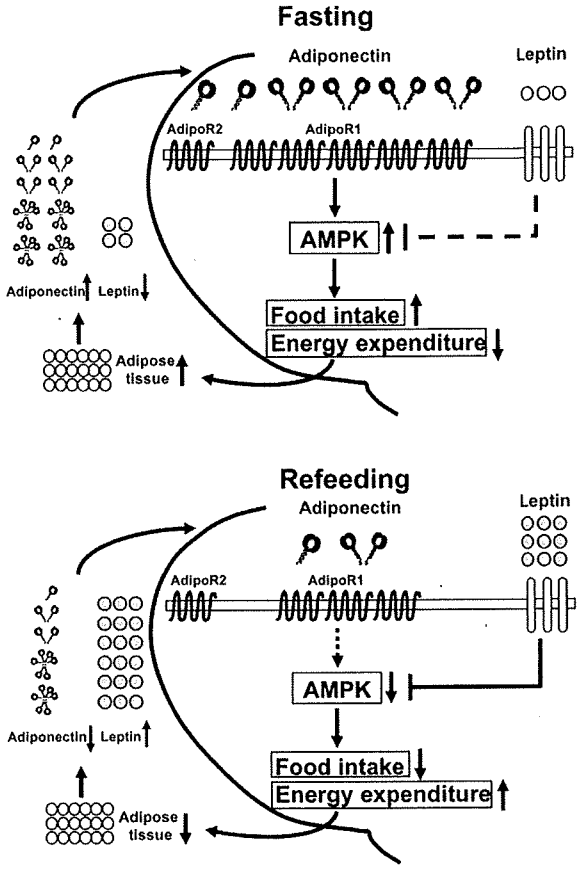

Figure 6. Adiponectin Regulates Food Intake and Energy Homeostasis

Under fasting conditions, serum and CSF adiponectin levels and AdipoR1 expression in the ARH increase; consequently, hypothalamic AMPK is activated, which stimulates food intake and suppresses energy expenditure, promoting fat storage. After refeeding, on the other hand, serum and CSF adiponectin levels and AdipoR1 expression in the ARH decrease; consequently, hypothalamic AMPK activity decreases, resulting in reduced food intake and increased energy expenditure. Serum leptin levels are regulated inversely in relation to serum adiponectin levels both under fasting conditions and after refeeding. Leptin suppresses hypothalamic AMPK activity and food intake, as opposed to the action of adiponectin. Thus, central adiponectin/leptin signals may represent the physiological pathway by which hypothalamic AMPK activity and food intake are stimulated under fasting conditions and suppressed by refeeding.

In summary, we propose a role for adiponectin in the regulation of AMPK activity in the hypothalamus, food intake, and energy expenditure. Our data also suggest that selective hypothalamic AdipoR1 antagonism may represent a novel therapeutic strategy for obesity and obesity-linked diseases.

EXPERIMENTAL PROCEDURES

Animals

Original *adipo*$^{-/-}$ mice (C57BL/6 and 129/Sv mixed background) (Kubota et al., 2002) were backcrossed with C57BL/6 mice more than seven times (Kubota et al., 2006). The mice were housed under a 12 hr light/dark cycle and given ad libitum access to food. Fasting, when needed, was started at the end of a light phase of the light/dark cycle. All experiments in this study were performed on male mice. Standard and HF (HF-32) diets were purchased from CLEA Japan, Inc. Long-term cannulae were implanted bilaterally into the ARH in designated groups of mice 7 days before the experiments were begun. Based on Franklin and Paxinos (1997), the stereotaxic coordinates for the intrahypothalamic injections were: anterior/posterior axis, 1.60 mm posterior to the bregma; lateral, ±0.5 mm from the midline; depth, 5.90 mm from the surface of the skull. Adenovirus vector (0.1 μl) expressing AdipoR1 siRNA (2.5×10^7 pfu/0.1 μl) (see below), AdipoR2 siRNA (2.5×10^7 pfu/0.1 μl) (see below), or D/N-AMPK (2.5×10^6 pfu/0.1 μl) (Minokoshi et al., 2004) was injected into the ARH bilaterally through the implanted cannulae. The control group was injected with adenovirus expressing LacZ (2.5×10^7 pfu/0.1 μl) (Yamauchi et al., 2003). Simultaneously, a catheter was inserted into the right jugular vein of all mice (see below). Body weight and food intake of all mice were monitored daily after the injections until completion of the experiments. Seven days after the injection of the adenovirus vector, saline, leptin (5 mg/kg), adiponectin (1 mg/kg), or leptin + adiponectin were administered via the catheter both under fasting conditions and after refeeding. In some groups (protocols 2 and 4), food intake was measured for 6 hr (Figures S3B and S3D), while in other groups (protocols 1 and 3), the animals were decapitated for sampling at 3 hr after the injections (Figures S3A and S3C). The ARH was quickly dissected from the first 1 mm-thick midline sagittal section of the brain, as described previously (Minokoshi et al., 2004), and frozen in liquid nitrogen. All animal care and experimental procedures conformed to the guidelines of the Animal Care Committee of the University of Tokyo.

Western Blot Analysis and Measurement of AMPK and ACC Phosphorylation

Tissues were excised and homogenized in ice-cold buffer A (25 mM Tris-HCl [pH 7.4], 10 mM sodium orthovanadate, 10 mM sodium pyrophosphate, 100 mM sodium fluoride, 10 mM EDTA, 10 mM EGTA, and 1 mM phenylmethylsulfonyl fluoride [PMSF]). The sample buffer for analysis under reducing conditions was composed of 3% SDS, 50 mM Tris-HCl (pH 6.8), 5% 2-mercaptoethanol, and 10% glycerol. Samples were mixed with 5× sample buffer, heated at 95°C for 5 min for heat denaturation, and then separated on polyacrylamide gels and transferred to a Hybond-P PVDF transfer membrane (Amersham Biosciences). Bands were detected with ECL detection reagents (Amersham Biosciences). For analysis under nonreducing conditions, 2-mercaptoethanol was excluded from the sample buffer described above. Serum samples were diluted 20-fold, while the CSF samples (2 μl) were used undiluted. Anti-mouse adiponectin antiserum was obtained by immunizing rabbits with mouse recombinant adiponectin globular domain produced in *E. coli* (Yamauchi et al., 2001). To detect the phosphorylation status of α2AMPK, lysates from the ARH (40–50 μg of protein) were immunoprecipitated with anti-phospho-AMPK (Cell Signaling Technology, Inc.) and blotted with an anti-α2AMPK antibody (Abgent). Lysates from the ARH (5–10 μg of protein) were blotted with anti-AMPK antibody (Cell Signaling Technology, Inc.) as a control. To detect the phosphorylation status of AMPK in skeletal muscle, lysates (20 μg of protein) were blotted with anti-phospho-AMPK (Cell Signaling Technology, Inc.) or with anti-AMPK (Cell Signaling Technology, Inc.) antibody as a control. To detect the phosphorylation status of ACC, lysates from the ARH (5–10 μg of protein) were blotted with anti-phospho-ACC (Upstate Biotechnology, Inc.) or with anti-ACC (Upstate Biotechnology, Inc.) antibody as a control. The AMPK and ACC phosphorylation data were normalized to the AMPK and ACC levels and calculated as the fold intensity relative to the baseline value and are representative of three independent experiments.

Generation of cRNA Probes and In Situ Hybridization

PCR products were ligated to the vector with a TA cloning kit (Invitrogen). ^{35}S-labeled riboprobes were generated from fragments of the PCR products for AdipoR1, AdipoR2, and the leptin receptor using a transcription kit according to the manufacturer's instructions (Boehringer Mannheim). Antisense probes for AdipoR1, AdipoR2, and the leptin receptor were generated using T3, T7, and Sp6 polymerases, respectively, and sense probes for all three were generated with Sp6/T7 polymerase (Ueta et al., 1995). Frozen 12 μm-thick mouse brain sections containing the hypothalamus were fixed in 4% formaldehyde; dehydrated by sequential transfer through 70%, 80%, 95%, and 100% ethanol; and delipidated in 100% chloroform for 5 min. The slides were hybridized with ^{35}S-labeled antisense and sense probes under Nescofilm coverslips, and the films were exposed for 3–8 days (Ueta et al., 1995). The data shown are representative of three independent experiments. White indicates the most intense signal, and black indicates the least intense signal.

Histological Analysis of WAT and Determination of Adipocyte Size

WAT was immediately immersion fixed overnight in Bouin's solution at 4°C. Tissues were routinely processed for paraffin embedding, and 2 μm sections were cut and mounted on silanized slides. The sections were stained with hematoxylin and eosin. The total area occupied by adipocytes was traced manually and analyzed with Win ROOF software (Mitani Co., Ltd.). The sizes of 200 or more white adipocytes per mouse in each group were determined as described previously (Kubota et al., 1999).

Generation of Adenoviral RNAi Constructs

The sequences of the sense siRNAs used were: mouse AdipoR1, 5′-AGACCAAATATGTACTTCATG-3′; mouse AdipoR2, 5′-CCCGACTCT TCTCTAAATTG-3′. An adenovirus vector expressing siRNA against AdipoR1 was constructed as described previously (Yamauchi et al., 2003), with minor modifications. The E1 and E3 regions of the circular form of adenoviral DNA were replaced with a cosmid vector flanked by FRT sites, designated as pAFC. The U6 promoter combined with the RNAi sequence and a loop sequence (TTCAAGAGA) was inserted into the SwaI site of pAFC between the FRT-flanked cosmid backbone and the adenoviral genome (Yamauchi et al., 2003). Cotransfection of an FLP expression plasmid with this cosmid into 293 cells efficiently excised the FRT-flanked cosmid vector backbone and produced an adenovirus vector expressing siRNA against AdipoR1 or AdipoR2. Prior to in vivo use, all adenovirus vectors were purified on a cesium chloride gradient and dialyzed with PBS plus 10% glycerol.

Immunohistochemistry for AdipoR1 and the Leptin Receptor in the Hypothalamus

AdipoR1 and the leptin receptor were visualized by immunohistochemical analysis in the hypothalamus. After PBS equilibration, 20 mm-thick frozen sections of hypothalamus were incubated with 3% normal goat serum in 2.5% Triton X-100/PBS as the blocking solution for 2 hr at room temperature. Simultaneous incubation with both primary anti-rabbit AdipoR1 antibody and anti-rat leptin receptor antibody diluted 1:100 was performed in blocking solution overnight at 4°C. After six washes with PBS, the slides were simultaneously incubated with both anti-rabbit IgG:Alexa Fluor 488 and anti-rat IgG:Alexa Fluor 546 (Molecular Probes) in blocking solution for 2 hr at room temperature. DAPI staining (1:200 dilution) was performed at room temperature for 5 min. After a final rinse with PBS, the sections were mounted with a ProLong Antifade kit (Molecular Probes) and examined under a fluorescence microscope (BZ-8000, Keyence) (Kondo et al., 2003).

Statistics

Data are expressed as ±SEM. Student's t test was used for statistical analysis of the differences between two groups, and the statistical significance of differences among multiple groups was determined by ANOVA and Tukey's t test.

Supplemental Data

Supplemental Data include Supplemental Experimental Procedures and four figures and can be found with this article online at http://www.cellmetabolism.org/cgi/content/full/6/1/55/DC1/.

ACKNOWLEDGMENTS

We thank H. Meguro, K. Takasawa, E. Yoshida-Nagata, N. Ohtsuka-Kowatari, A. Nagano, M. Nakashima, N. Kasuga, Y. Miki, and H. Chiyonobu for providing excellent technical assistance and animal care. This work was supported by a Grant-in-Aid for Creative Scientific Research from the Japan Society for the Promotion of Science (10NP0201), a grant from the Juvenile Diabetes Foundation International (1-2003-746), a Grant-in-Aid for the Development of Innovative Technology from the Ministry of Education, Culture, Sports, Science and Technology of Japan, Health Science Research grants (Research on Human Genome and Gene Therapy) from the Ministry of Health and Welfare, a grant for Promotion of Fundamental Studies in Health Science of the Organization for Pharmaceutical Safety and Research (to T. Kadowaki), a grant for Life & Socio-Medical Sciences from the Kanae Foundation, a grant from the Sankyo Foundation of Life Science, and a grant from Astellas Foundation for Research on Metabolic Disorders (to N.K.).

Received: January 12, 2007
Revised: April 26, 2007
Accepted: June 14, 2007
Published: July 10, 2007

REFERENCES

Andersson, U., Filipsson, K., Abbott, C.R., Woods, A., Smith, K., Bloom, S.R., Carling, D., and Small, C.J. (2004). AMP-activated protein kinase plays a role in the control of food intake. J. Biol. Chem. *279*, 12005–12008.

Berg, A.H., Combs, T.P., Du, X., Brownlee, M., and Scherer, P.E. (2001). The adipocyte-secreted protein Acrp30 enhances hepatic insulin action. Nat. Med. *7*, 947–953.

Carling, D. (2005). AMP-activated protein kinase: balancing the scales. Biochimie *87*, 87–91.

Franklin, K.B.J., and Paxinos, G. (1997). The Mouse Brain in Stereotaxic Coordinates (San Diego, CA, USA: Academic Press).

Fruebis, J., Tsao, T.S., Javorschi, S., Ebbets-Reed, D., Erickson, M.R., Yen, F.T., Bihain, B.E., and Lodish, H.F. (2001). Proteolytic cleavage product of 30-kDa adipocyte complement-related protein increases fatty acid oxidation in muscle and causes weight loss in mice. Proc. Natl. Acad. Sci. USA *98*, 2005–2010.

Hada, Y., Yamauchi, T., Waki, H., Tsuchida, A., Hara, K., Yago, H., Miyazaki, O., Ebinuma, H., and Kadowaki, T. (2007). Selective purification and characterization of adiponectin multimer species from human plasma. Biochem. Biophys. Res. Commun. *356*, 487–493.

Hardie, D.G. (2004). The AMP-activated protein kinase pathway–new players upstream and downstream. J. Cell Sci. *117*, 5479–5487.

Kadowaki, T., Yamauchi, T., Kubota, N., Hara, K., Ueki, K., and Tobe, K. (2006). Adiponectin and adiponectin receptors in insulin resistance, diabetes, and the metabolic syndrome. J. Clin. Invest. *116*, 1784–1792.

Kahn, C.R. (2000). Triglycerides and toggling the tummy. Nat. Genet. *25*, 6–7.

Karpichev, I.V., Cornivelli, L., and Small, G.M. (2002). Multiple regulatory roles of a novel Saccharomyces cerevisiae protein, encoded by YOL002c, in lipid and phosphate metabolism. J. Biol. Chem. *277*, 19609–19617.

Kim, J.-Y., van de Wall, E., Laplante, M., Azzara, A., Trujillo, M.E., Hofmann, S.M., Schraw, T., Durand, J.L., Li, H., Li, G., et al. (2007). Obesity-associated improvements in metabolic profile in mice: rescue of the diabetic phenotype through expansion of adipose tissue mass. J. Clin. Invest., in press.

Kim, M.S., and Lee, K.U. (2005). Role of hypothalamic 5′-AMP-activated protein kinase in the regulation of food intake and energy homeostasis. J. Mol. Med. *83*, 514–520.

Kondo, T., Vicent, D., Suzuma, K., Yanagisawa, M., King, G.L., Holzenberger, M., and Kahn, C.R. (2003). Knockout of insulin and IGF-1 receptors on vascular endothelial cells protects against retinal neovascularization. J. Clin. Invest. *111*, 1835–1842.

Kos, K., Harte, A.L., da Silva, N.F., Tonchev, A., Chaldakov, G., James, S., Snead, D.R., Hoggart, B., O'Hare, J.P., McTernan, P.G., et al. (2007). Adiponectin and resistin in human cerebrospinal fluid and expression of adiponectin receptors in the human hypothalamus. J. Clin. Endocrinol. Metab. *92*, 1129–1136.

Kubota, N., Terauchi, Y., Miki, H., Tamemoto, H., Yamauchi, T., Komeda, K., Satoh, S., Nakano, R., Ishii, C., Sugiyama, T., et al. (1999). PPAR gamma mediates high-fat diet-induced adipocyte hypertrophy and insulin resistance. Mol. Cell *4*, 597–609.

Kubota, N., Terauchi, Y., Yamauchi, T., Kubota, T., Moroi, M., Matsui, J., Eto, K., Yamashita, T., Kamon, J., Satoh, H., et al. (2002). Disruption of adiponectin causes insulin resistance and neointimal formation. J. Biol. Chem. *277*, 25863–25866.

Kubota, N., Terauchi, Y., Kubota, T., Kumagai, H., Itoh, S., Satoh, H., Yano, W., Ogata, H., Tokuyama, K., Takamoto, I., et al. (2006). Pioglitazone ameliorates insulin resistance and diabetes by both adiponectin-dependent and -independent pathways. J. Biol. Chem. *281*, 8748–8755.

Kusminski, C.M., McTernan, P.G., Schraw, T., Kos, K., O'hare, J.P., Ahima, R., Kumar, S., and Scherer, P.E. (2007). Adiponectin complexes in human cerebrospinal fluid: distinct complex distribution from serum. Diabetologia *50*, 634–642.

Luo, Z., Saha, A.K., Xiang, X., and Ruderman, N.B. (2005). AMPK, the metabolic syndrome and cancer. Trends Pharmacol. Sci. *26*, 69–76.

Minokoshi, Y., Kim, Y.B., Peroni, O.D., Fryer, L.G., Muller, C., Carling, D., and Kahn, B.B. (2002). Leptin stimulates fatty-acid oxidation by activating AMP-activated protein kinase. Nature *415*, 339–343.

Minokoshi, Y., Alquier, T., Furukawa, N., Kim, Y.B., Lee, A., Xue, B., Mu, J., Foufelle, F., Ferre, P., Birnbaum, M.J., et al. (2004). AMP-kinase regulates food intake by responding to hormonal and nutrient signals in the hypothalamus. Nature *428*, 569–574.

Nawrocki, A.R., Rajala, M.W., Tomas, E., Pajvani, U.B., Saha, A.K., Trumbauer, M.E., Pang, Z., Chen, A.S., Ruderman, N.B., Chen, H., et al. (2006). Mice lacking adiponectin show decreased hepatic insulin sensitivity and reduced responsiveness to peroxisome proliferator-activated receptor gamma agonists. J. Biol. Chem. *281*, 2654–2660.

Pajvani, U.B., Du, X., Combs, T.P., Berg, A.H., Rajala, M.W., Schulthess, T., Engel, J., Brownlee, M., and Scherer, P.E. (2003). Structure-function studies of the adipocyte-secreted hormone Acrp30/adiponectin. Implications for metabolic regulation and bioactivity. J. Biol. Chem. *278*, 9073–9085.

Qi, Y., Takahashi, N., Hileman, S.M., Patel, H.R., Berg, A.H., Pajvani, U.B., Scherer, P.E., and Ahima, R.S. (2004). Adiponectin acts in the brain to decrease body weight. Nat. Med. *10*, 524–529.

Scherer, P.E. (2006). Adipose tissue: from lipid storage compartment to endocrine organ. Diabetes *55*, 1537–1545.

Scherer, P.E., Williams, S., Fogliano, M., Baldini, G., and Lodish, H.F. (1995). A novel serum protein similar to C1q, produced exclusively in adipocytes. J. Biol. Chem. *270*, 26746–26749.

Schwartz, M.W., and Porte, D., Jr. (2005). Diabetes, obesity, and the brain. Science *307*, 375–379.

Spranger, J., Verma, S., Gohring, I., Bobbert, T., Seifert, J., Sindler, A.L., Pfeiffer, A., Hileman, S.M., Tschop, M., and Banks, W.A. (2006). Adiponectin does not cross the blood-brain barrier but modifies cytokine expression of brain endothelial cells. Diabetes *55*, 141–147.

Ueta, Y., Levy, A., Chowdrey, H.S., and Lightman, S.L. (1995). S-100 antigen-positive folliculostellate cells are not the source of IL-6 gene expression in human pituitary adenomas. J. Neuroendocrinol. *7*, 467–474.

Xue, B., and Kahn, B.B. (2006). AMPK integrates nutrient and hormonal signals to regulate food intake and energy balance through effects in the hypothalamus and peripheral tissues. J. Physiol. *574*, 73–83.

Yamauchi, T., Kamon, J., Waki, H., Terauchi, Y., Kubota, N., Hara, K., Mori, Y., Ide, T., Murakami, K., Tsuboyama-Kasaoka, N., et al. (2001). The fat-derived hormone adiponectin reverses insulin resistance associated with both lipoatrophy and obesity. Nat. Med. *7*, 941–946.

Yamauchi, T., Kamon, J., Minokoshi, Y., Ito, Y., Waki, H., Uchida, S., Yamashita, S., Noda, M., Kita, S., Ueki, K., et al. (2002). Adiponectin stimulates glucose utilization and fatty-acid oxidation by activating AMP-activated protein kinase. Nat. Med. *8*, 1288–1295.

Yamauchi, T., Kamon, J., Ito, Y., Tsuchida, A., Yokomizo, T., Kita, S., Sugiyama, T., Miyagishi, M., Hara, K., Tsunoda, M., et al. (2003). Cloning of adiponectin receptors that mediate antidiabetic metabolic effects. Nature *423*, 762–769.

Yamauchi, T., Nio, Y., Maki, T., Kobayashi, M., Takazawa, T., Iwabu, M., Okada-Iwabu, M., Kawamoto, S., Kubota, N., Kubota, T., et al. (2007). Targeted disruption of AdipoR1 and AdipoR2 causes abrogation of adiponectin binding and metabolic actions. Nat. Med. *13*, 332–339.

Zlokovic, B.V., Jovanovic, S., Miao, W., Samara, S., Verma, S., and Farrell, C.L. (2000). Differential regulation of leptin transport by the choroid plexus and blood-brain barrier and high affinity transport systems for entry into hypothalamus and across the blood-cerebrospinal fluid barrier. Endocrinology *141*, 1434–1441.

BASIC RESEARCH www.jasn.org

Role of Altered Renal Lipid Metabolism in the Development of Renal Injury Induced by a High-Fat Diet

Shinji Kume,* Takashi Uzu,* Shin-ichi Araki,* Toshiro Sugimoto,* Keiji Isshiki,* Masami Chin-Kanasaki,* Masayoshi Sakaguchi,* Naoto Kubota,† Yasuo Terauchi,‡ Takashi Kadowaki,† Masakazu Haneda,§ Atsunori Kashiwagi,* and Daisuke Koya*‖

*Department of Medicine, Shiga University of Medical Science, Otsu, Shiga, †Department of Metabolic Diseases, Graduate School of Medicine, University of Tokyo, Tokyo, ‡Department of Endocrinology and Metabolism, Yokohama City University Graduate School of Medicine, Yokohama, §Second Department of Medicine, Asahikawa Medical College, Asahikawa, Hokkaido, and ‖Division of Endocrinology & Metabolism, Kanazawa Medical University, Kahoku-Gun, Ishikawa, Japan

ABSTRACT

Metabolic syndrome is associated with increased risk of chronic kidney disease, and the renal injury in patients with metabolic syndrome may be a result of altered renal lipid metabolism. We fed wild-type or insulin-sensitive heterozygous peroxisome proliferator–activated receptor γ–deficient ($PPAR\gamma^{+/-}$) mice a high-fat diet for 16 weeks. In wild-type mice, this diet induced core features of metabolic syndrome, subsequent renal lipid accumulation, and renal injury including glomerulosclerosis, interstitial fibrosis, and albuminuria. Renal lipogenesis accelerated, determined by increased renal mRNA expression of the lipogenic enzymes fatty acid synthase and acetyl-CoA carboxylase (ACC) and by increased ACC activity. In addition, renal lipolysis was suppressed, determined by reduced mRNA expression of the lipolytic enzyme carnitine palmitoyl acyl-CoA transferase 1 and by reduced activity of AMP-activated protein kinase. In $PPAR\gamma^{+/-}$ mice, renal injury, systemic metabolic abnormalities, renal accumulation of lipids, and the changes in renal lipid metabolism were attenuated. Thus, a high-fat diet leads to an altered balance between renal lipogenesis and lipolysis, subsequent renal accumulation of lipid, and renal injury. We suggest that renal lipid metabolism could serve as a new therapeutic target to prevent chronic kidney disease in patients with metabolic syndrome.

J Am Soc Nephrol 18: 2715–2723, 2007. doi: 10.1681/ASN.2007010089

Metabolic syndrome, which is characterized by concurrent existence of obesity, dyslipidemia, hyperinsulinemia, hyperglycemia, and hypertension, is increasingly common because of increased prevalence of obesity. This syndrome is a growing health problem because of the associated increased risk for cardiovascular disease and premature death.[1,2] Furthermore, a recent report suggested that individuals with metabolic syndrome are also at increased risk for developing chronic kidney diseases (CKD).[3]

Several pathomechanisms underlying the development of renal injury in metabolic syndrome have been proposed.[4–8] Among them, renal lipid accumulation, lipotoxicity, has been reported to play an important role in the pathogenesis of renal injury in metabolic syndrome, although the precise mechanism of renal lipid accumulation has not been fully

Received January 23, 2007. Accepted June 7, 2007.

Published online ahead of print. Publication date available at www.jasn.org.

Correspondence: Dr. Daisuke Koya, Division of Endocrinology & Metabolism, Kanazawa Medical University, Kahoku-Gun, Ishikawa 920-0293, Japan. Phone: +81-76-286-2211; Fax: +81-76-286-6927; E-mail: koya0516@kanazawa-med.ac.jp